SMC-TR-98-37

AEROSPACE REPORT NO.
TR-98(1410)-2

Ground Cloud Dispersion Measurements During The Titan IV Mission #K15 (5 December 1995) at Vandenberg Air Force Base

Volume 2—Further Analysis of Quantitative Imagery and of Aircraft HCl Data

12 May 1998

Prepared by

R. N. ABERNATHY and K. L. FOSTER
Space and Environment Technology Center
Technology Operations

Prepared for

SPACE AND MISSILE SYSTEMS CENTER
AIR FORCE MATERIEL COMMAND
2430 E. El Segundo Boulevard
Los Angeles Air Force Base, CA 90245

Space Systems Group

THE AEROSPACE CORPORATION
El Segundo, California

This report was submitted by The Aerospace Corporation, El Segundo, CA 90245-4691, under Contract No. F04701-93-C-0094 with the Space and Missile Systems Center, 2430 E. El Segundo Blvd., Los Angeles Air Force Base, CA 90245. It was reviewed and approved for The Aerospace Corporation by A. B. Christensen, Principal Director, Space and Environment Technology Center. Capt. W. Kempf was the project officer.

This report has been reviewed by the Public Affairs Office (PAS) and is releasable to the National Technical Information Service (NTIS). At NTIS, it will be available to the general public, including foreign nationals.

This technical report has been reviewed and is approved for publication. Publication of this report does not constitute Air Force approval of the report's findings or conclusions. It is published only for the exchange and stimulation of ideas.

Capt. William Kempf
SMC/CLTE

REPORT DOCUMENTATION PAGE

Form Approved
OMB No. 0704-0188

1. AGENCY USE ONLY (*Leave blank*)	2. REPORT DATE	3. REPORT TYPE AND DATES COVERED
	12 May 1998	

4. TITLE AND SUBTITLE
Ground Cloud Dispersion Measurements During The Titan IV Mission #K15 (5 Dec 1995) at Vandenberg Air Force Base: Vol 2—Further Analysis of Quantitative Imagery and of Aircraft HCl Data

5. FUNDING NUMBERS
F04701-93-C-0094

6. AUTHOR(S)
R. N. Abernathy and K. L. Foster

7. PERFORMING ORGANIZATION NAME(S) AND ADDRESS(ES)
The Aerospace Corporation
Technology Operations
El Segundo, CA 90245-4691

8. PERFORMING ORGANIZATION REPORT NUMBER
TR-98(1410)-2

9. SPONSORING/MONITORING AGENCY NAME(S) AND ADDRESS(ES)
Space and Missile Systems Center
Air Force Materiel Command
2430 E. El Segundo Boulevard
Los Angeles Air Force Base, CA 90245

10. SPONSORING/MONITORING AGENCY REPORT NUMBER
SMC-TR-98-37

11. SUPPLEMENTARY NOTES

12a. DISTRIBUTION/AVAILABILITY STATEMENT
Approved for public release; distribution unlimited

12b. DISTRIBUTION CODE

13. ABSTRACT (*Maximum 200 words*)

The atmospheric dispersion Model Validation Program (MVP) collects and distributes launch cloud dispersion and transport data for the launch community. A previous report provided an overview and data summary for launch cloud measurements associated with the Titan IV Mission #K15 launch (5 December 1995). This report presents a more detailed analysis, both for the aircraft HCl measurements and for the quantitative imagery. This analysis includes a comparison, at one-min resolution, of the aircraft's HCl sampling data with the results of simultaneous quantitative imagery. The combined data provide a three-dimensional perspective of the solid rocket motor exhaust cloud for the first 11 min after launch. In addition, this report provides a detailed graphical plotting of the aircraft's HCl measurements and maps the HCl concentrations both in time and in space. Comparisons reveal that both REEDM version 7.07 and version 7.08 predict lower-than-measured HCl concentrations at the predicted stabilization height. These aircraft data document fragmentation of the cloud into separate parcels and slower-than-expected dispersion of these portions of the ground cloud. The imagery data documented the rise and stabilization of the cloud during the first 11 min after launch. These data are useful for quantifying the accuracy of the Rocket Exhaust Effluent Diffusion Model (REEDM) as it is tuned for better agreement with measured cloud characteristics.

14. SUBJECT TERMS	15. NUMBER OF PAGES
Toxic launch cloud, Toxic hazard corridor, Atmospheric dispersion model, Launch cloud development and dispersion, Launch cloud imagery, HCl monitoring, Titan IV	56
	16. PRICE CODE

17. SECURITY CLASSIFICATION OF REPORT	18. SECURITY CLASSIFICATION OF THIS PAGE	19. SECURITY CLASSIFICATION OF ABSTRACT	20. LIMITATION OF ABSTRACT
UNCLASSIFIED	UNCLASSIFIED	UNCLASSIFIED	

Acknowledgments

The Air Force Space and Missile Systems Center's Launch Programs Office (SMC/CLNER) is sponsoring the Atmospheric Dispersion Model Validation Program (MVP). This program is collecting launch cloud dispersion data that will be used to determine the accuracy of atmospheric dispersion models, such as REEDM, in predicting toxic hazard corridors at the launch ranges. This report correlates quantitative launch cloud imagery with aircraft HCl measurements performed during the Titan IV Mission #K15 at Vandenberg Air Force Base on 5 December 1995. These results are compared to REEDM version 7.07 and 7.08 predictions.

An MVP Integrated Product Team (IPT) led by Capt. Brian Laine (SMC/CLNER) is directing the MVP effort. Dr. Bart Lundblad of The Aerospace Corporation's Environmental Systems Directorate (ESD) is the MVP technical manager.

Visible and infrared (IR) imagery measurements were made of the launch cloud by Dr. Robert N. Abernathy, Ms. Karen L. Foster, Mr. Robert A. Klingberg, J. Y. Webb, Dr. J. Tom Knudtson, and Dr. George J. Scherer of The Aerospace Corporation's Surveillance Technology Department (STD). Mr. J. F. Kephart of The Aerospace Corporation's Western Range Directorate coordinated site selection and logistical support with Range organizations. Ms. Foster digitized imagery data for analysis by Dr. Abernathy. Mr. Kasper created and maintains the PLMTRACK program used by Dr. Abernathy for pairwise analysis of simultaneously acquired imagery from two sites. Ms. Foster performed the graphical comparison of the imagery results against the aircraft HCl measurements. Dr. Abernathy prepared the description of the cloud imagery results and analysis.

The aircraft-based HCl measurement effort was managed by Mr. Marv Becker and Mr. Pete Mazur of SRS Technologies. The Piper Seminole sampling aircraft was owned and operated by Florida Institute of Technology. The aircraft was outfitted with a Geomet HCl detector that was modified and calibrated for airborne sampling by Mr. Paul Yocom of the NASA Toxic Vapor Detection/Contamination Monitoring Laboratory. Ms. Jeanne Hawkins of the 45th Medical Group Bioenvironmental Engineering Services (45 AMDS/SGPB) was on-board the aircraft during the sampling measurements to monitor Geomet performance and cockpit contamination. The on-board data logger and GPS system was provided and installed by Mr. Shane Beard of NOAA's Environmental Research Laboratories. The Spectral Sciences IR HCl detector was installed and managed by Dr. Steve Richtsmeier of Spectral Sciences, INC. The raw IR HCl detector data were processed and analyzed by Drs. Abernathy and Richtsmeier. The raw Geomet HCl detector data were processed and analyzed by Dr. Abernathy and Ms. Foster. Ms. Foster performed the graphical comparison of the imagery results against the aircraft HCl measurements. Dr. Abernathy analyzed the response characteristics and calibration of the Geomet and compared the Geomet's HCl data to the HCl data from the faster IR detector. Dr. Abernathy prepared the description of the aircraft sampling and cloud imagery results.

The ground-level HCl measurements effort was managed by Lt. Col. Kent Stringham of the 30th Medical Group Bioenvironmental Engineering Services organization (30 AMDS/SGPB). The HCl dosimeters were provided by and later analyzed by the NASA Toxic Vapor Detection/Contamination Monitoring Laboratory. The ground-level HCl measurements were discussed in Volume 1 and are not discussed in this report.

The meteorological data were provided by Mr. Steve Sambol of the VAFB Weather Squadron (30WS/DOS). The REEDM launch cloud dispersion prediction was provided by Mr. Darryl Dargitz of the VAFB Range Safety Office (30 SW/SEY). See the Volume 1 report for these data.

The #K15 mission was the fifth Titan IV launch for which usable launch cloud dispersion data were collected by MVP. The previous missions were #K7, #K23, #K19, and #K21. It was the second Titan IV launch to employ an aircraft to collect HCl dispersion data. The previous airborne sampling activity was following the #K23 launch. The MVP continues to collect cloud dispersion data as needed to validate current and future models.

Contents

Figures

Tables

Executive Summary

A previous report presented an overview and data summary for ground cloud dispersion measurements during the Titan IV mission #K15 launch from VAFB on 5 December 1995. That report documented the instrumentation, methods of analysis, and preliminary results for the program. The preliminary results included the following: (1) the imagery-derived cloud speed, direction, and position for the first 11 min after launch; (2) the aircraft-derived cloud bearing and altitude-dependent extent for the first 100 min after launch; and (3) comparison of imagery-derived, aircraft-derived, rawinsonde-derived data to REEDM version 7.07 predictions. This second report provides a detailed comparison of the imagery-derived extent of the ground cloud to simultaneous aircraft sampling data. The combined data provides a three-dimensional perspective of the exhaust cloud during the first 11 min after launch. In addition, this report includes a more detailed graphing and analysis of the aircraft's HCl measurements. This processing enabled direct comparison to REEDM version 7.07 and 7.08 dispersion model predictions.

The #K15 imagery and aircraft data document substantial differences between measured and predicted cloud characteristics. REEDM version 7.08 and REEDM version 7.07 substantially underestimate the maximum HCl concentrations at the stabilization height at times greater than 40 min (i.e., distances greater than 25 km). The magnitude of the errors are substantial (i.e., 2 to 14 ppm low) representing minimal errors of -80 to -90% (i.e., predicted values are only 10 to 20% of measured values) by 100 min after launch. Discussions document that any bias in the Geomet's HCl measurements would only increase the difference between actual HCl concentrations and predicted HCl concentrations. The data suggest that the exhaust cloud fragments into parcels that disperse more slowly than predicted. The imagery documented the stabilization time and heights for the #K15 exhaust cloud and, when combined with the aircraft's HCl data, will be useful for validating REEDM as it is tuned for better agreement with measurements.

The analyzed data for the Titan IV mission #K15 is one part of a larger dataset. Dispersion models must account for many variables that include the following: the effect of terrain (i.e., Eastern and Western launch ranges); weather conditions (i.e., wind speed, wind shear, cloud cover, humidity, rain); daily variations (i.e., solar angle and sea breeze conditions); and seasonal variations (i.e., solar angle and meteorology). Therefore, the MVP is acquiring ground cloud dispersion data at both ranges, at various times of day (and night), and during various seasons. The #K15 mission is the fifth Titan IV mission for which useable launch cloud dispersion data were collected by MVP. The #K15 mission is the second Titan IV launch to employ an aircraft to collect HCl dispersion data. These data are being used to test dispersion models and have already been the motivation for several proposed modifications to the REEDM.

1. Introduction

Dispersion model predictions have delayed launches from both Cape Canaveral Air Station (CCAS) and Vandenberg Air Force Base (VAFB). Delays occur when the predicted concentrations of toxic gases resulting from a normal or an aborted launch exceed public exposure criteria. The Rocket Exhaust Effluent Dispersion Model (REEDM) predicts the downwind concentrations of toxic gases for various launch vehicles (e.g., Shuttle, Titan, and Delta) for the normal and several abort scenarios. REEDM predictions are deliberately conservative to compensate for uncertainties in the modeling physics. Therefore, it is desirable to validate the performance of such dispersion models against actual launch cloud dispersion and transport data.

The Air Force launch range safety organizations of the 45th Space Wing at Patrick Air Force Base (45 SW/SE) and the 30th Space Wing at VAFB (30 SW/SE) are responsible for assuring that launches are carried out only when meteorological conditions are such that nearby communities cannot be exposed to hazardous levels of HCl, the hydrazine fuels, or N_2O_4/NO_2. Predictions of toxic hazard corridors (THCs) that extend into public areas can lead to costly launch delays. Presently, safety concerns mandate a conservative interpretation of model predictions since the models have not been fully validated. Thus, development and validation of accurate atmospheric dispersion models is expected to increase launch opportunities and thereby reduce launch costs.

1.1 Model Validation Program

The Space and Missile System Center's Launch Programs Office (SMC/CLNER) established the Atmospheric Dispersion Model Validation Program (MVP). MVP is collecting the data necessary to determine the accuracy of current and future atmospheric dispersion and chemical kinetic models in predicting THCs during launches of Titan and other vehicles at CCAS and VAFB.

Model validation requires a complete set of cloud dispersion and transport data as well as any ancillary data needed as input to current or future dispersion models. Therefore, the MVP effort involves not only the collection of launch cloud data (i.e., HCl concentration profiles, cloud rise rates, cloud expansion rates, cloud speed, and cloud direction) but also the collection of meteorological data (i.e., rawinsonde soundings, Doppler acoustic sounder profiles, solar radiance data, terrain maps, and meteorological tower data). In addition to monitoring launch clouds, MVP involves measurements against tracer gas releases that provide not only a better definition of the source term (i.e., release altitude and geometry) but also optimization of the dataset (i.e., release conditions can be tuned for maximum overlap with sensor systems or with target land masses). Therefore, the MVP data will provide the needed test cases to validate current and future dispersion, transport, and chemical kinetic models.

The Aerospace Corporation has been deploying visible and/or IR imaging systems to Titan IV launches since the #K10 launch on 07 February 1994. The deployments in behalf of the MVP include Titan IV missions #K02, #K07, #K09, #K10, #K13, #K14, #K15, #K16, #A17, #A18, #K19,

#K21, #K22, #K23, #B24, and #B33. Typically, two-dimensional cloud images are recorded at each of two to three imaging sites and are combined in a pairwise fashion to produce stereoscopic 3-D information about the exhaust cloud. When atmospheric conditions were favorable and two (or more) imagery sites were manned (i.e., #K02, #K07, #K13, #K15, #K16, #A17, #A18, #K19, #K21, #K22, #K23, #B24, and #B33), the analysis of these data yields the ground cloud's rise time, stabilization height, dimensions, ground track, and ground speed. These imagery data and the resulting cloud characteristics are available to modelers as part of the MVP.[1-8]

The MVP has deployed aircraft to collect HCl concentration data to Titan IV launches #K23,[1] #K15,[4] #K16,[5] and #K22.[6] Typically, the aircraft's near-field HCl concentration profiles are interpreted using the simultaneously acquired imagery. The combined data[8] provides a 3-D perspective of the cloud by documenting the portion of the cloud sampled by the aircraft based upon the imagery-derived extent of the cloud and the concentration profile within that portion of the cloud. At later times, the aircraft's HCl concentration profiles[9] document the trajectory followed by the cloud and the decrease in peak HCl concentration as it moves away from the range. These aircraft HCl concentration data are available to modelers as part of the MVP.[1,4,5,6,8,9]

1.2 #K15 Ground Cloud Measurements

The Titan IV #K15 mission was launched successfully from the Western Range (i.e., from SLC-4E) at 13:18 PST (21:18 ZULU) on 5 December 1995. Personnel from The Aerospace Corporation deployed one IR imaging system and three visible imagery systems to monitor this daylight launch and to track the time evolution and the ground trajectory of the solid rocket motor exhaust cloud. Exhaust cloud imagery data were collected from three imagery sites during the 30 min immediately following the launch. The imagery sites used for the #K15 launch were the Tetra Tech Gravel Pit (northeast of SLC-4E on 13th Street), Building 900 (north-northeast of SLC-4E on Mesa Road), and Block Wall Beach (North of SLC-4E on Beach Road). A modified Geomet total hydrochloric acid (HCl) detector was mounted in the nose of a Piper (PA-44-180) Seminole, twin-engine, four-seat aircraft. The Geomet measured the combined aerosol and gaseous HCl concentration during the first 100 min after the #K15 launch. A Spectral Sciences IR HCl detector was mounted below the Piper Seminole and measured HCl vapor for the first few encounters with the exhaust cloud. This aircraft sampling campaign involved Air Force, NASA, NOAA, and contractor (I-NET, SRS, and Spectral Sciences) organizations. The Aerospace Corporation analyzed the aircraft's HCl concentration data and the ground-based imagery as described in a previous report.[4]

1.2.1 Previously Reported Results of Quantitative Imagery

As presented in the previous report,[4] the initial analysis of the imagery data focused on determining parameters that were directly comparable to REEDM version 7.07 predictions using default input parameters (i.e., tabulated later in this report). For quantitative imagery, the most accurately determined quantities are the cloud's rise time, its stabilization height, the cloud's speed, and its ground track. In addition, the imagery documented the rate of growth in the size of the #K15 exhaust cloud. Using the T-0.25h rawinsonde data, REEDM predicted a stabilization height of 514 m above ground level and a stabilization time of 2.8 min while the imagery yielded values of 658 m above SLC-4E and 3-5 min. The imagery-derived cloud trajectory was 8° and the cloud's ground speed was 9.2 m/s away from SLC-4E. This compares to 344° and 7.6 m/s predicted by REEDM (T-0.25h). Therefore,

the imaged cloud stabilized at a height that was 28% higher than predicted by REEDM (T-0.25h), traveled at a speed 21% faster than predicted by REEDM (T-0.25h), and headed in a direction 24° more clockwise than predicted by REEDM (T-0.25h).

1.2.2 Previously Reported Results of Aircraft HCl Measurements

The aircraft's Geomet total HCl detector sampled the ground cloud from the Titan IV #K15 launch and obtained a large quantity of HCl concentration data as a function of time and aircraft position. The aircraft's HCl concentration data documented a shifting trajectory for the aircraft's encounters with the ground cloud. At early times (4-20 min), the aircraft encounters fell along a southerly trajectory that was consistent with the imagery-derived cloud track and with REEDM's prediction for the rising ground cloud. At later times, the aircraft encounters shifted towards the southeast, which was consistent with REEDM's prediction for times after stabilization. This trend was reproduced by aircraft sampling at various altitudes between 400 and 1000 m MSL by GPS. For comparison, the imagery-derived altitudes for the bottom, middle, and top of the ground cloud were 536, 811, and 1327 m MSL along a southerly track. Therefore, most of the aircraft's HCl measurements were at altitudes within the stabilized ground cloud (as defined by imagery during the first 11 min after launch). One should remember three things when comparing the aircraft and imagery data: (1) the GPS altitude could be off by ±250 m, (2) the aircraft sampled for longer times than available by imagery, and (3) the aircraft did not probe the widest portion of the cloud. In fact, at later times, the aircraft sampled only a small portion of the cloud that moved to the southeast. The aircraft also sampled at altitudes below 400 m MSL according to its GPS receiver. These low-altitude data document an apparent shift in cloud trajectory below 400 m. These data suggest that the lowest-altitude portion of the ground cloud moved to the southeast faster than the bulk of the ground cloud (i.e., above 400 m MSL by GPS). Again, one must remember that the aircraft search pattern probably sampled only a portion of the cloud and may mislead the analyst. The aircraft's data document measurable levels of HCl to altitudes as low as 150 m MSL by GPS. The aircraft's data include HCl detection at times greater than 95 min after the launch and as great as 60 km from SLC-4E.

The aircraft's Geomet data (i.e., total HCl concentration measurements) were reported in several graphical formats to facilitate comparison with REEDM predictions (Appendix A[4]), rawinsonde sounding data (Appendix B[4]), gaseous HCl measurements (Chapter 4[4]), and imagery data (Chapter 2[4]). The aircraft setup was described in Appendix C.[4] The purpose of the earlier report[4] was to document the quality and quantity of the aircraft data available for validating dispersion models. However, it would be difficult to extract the data for a single pass through the cloud from summary plots that contain 41 passes through the cloud. Therefore, this report provides the data in a more detailed graphical form that should allow direct comparison to model predictions.

The Geomet detector appears to be useful for aircraft sampling of launch clouds. The previous report[4] provided data that illustrated quantitative integrated response as well as excellent temporal and spatial accuracy for mapping the extent and position of Titan IV clouds. Those data also documented significant differences in the HCl concentrations reported by the Geomet and another detector that flew on this mission. It was illustrated that the concentration reported by both detectors is a strong function of their response functions (i.e., averaging time).

It was suggested that the Geomet reports an HCl concentration that represents an average value for at least an 18 s averaging time.[4] In contrast, the temporal and spatial accuracy of the Geomet is consistent with an averaging time of only 3 to 4 s.[4] Therefore, we recommend the use of caution when comparing measured HCl concentration to predicted HCl concentration since the averaging times associated with the detector are not the same as those used in typical dispersion model runs. In our comparisons, we document that the Geomet's measured HCl concentration was greater than REEDM's predicted instantaneous concentration (i.e., no averaging). Certainly, the Geomet's values must be lower than the actual HCl concentrations. Therefore, the actual differences between the #K15 exhaust cloud HCl concentration and the REEDM prediction are greater than observed.

The previous analysis also discovered an error in the REEDM output while comparing the REEDM predictions to imagery-derived and aircraft-derived altitude-dependent measurements. REEDM converts the height above ground level (AGL) to height above mean sea level (MSL) by using the height of the rawinsonde release site (112 m, 368 ft,) instead of the height of launch pad (153 m, 501 ft). Therefore, the height MSL reported by REEDM in Appendix A[4] is 41 m (133 ft) too low (i.e., 153m–112m).

1.2.3 Additional Analysis Included in This Report

This report extends the analysis of the #K15 ground cloud measurements by comparing the results of the aircraft's HCl measurements to the imagery-derived extent of the exhaust cloud. This comparison correlates the aircraft's HCl measurements with the imagery for the first 11 min after launch to document the dimensions and concentration distributions within the rising and the stabilized ground cloud. A similar comparison was reported previously for the #K23 ground cloud measurements.[8] This report also documents the aircraft's measurements of the #K15 ground cloud's HCl concentrations to greater spatial and temporal resolution than covered in the test overview.[4] The detailed graphical analysis of the aircraft's HCl concentrations includes profiles using polar and Cartesian coordinates for each 10-min time window for the first 100 min after launch. In addition to cloud concentrations, one can extract angular spreads and along-wind cloud dimensions for favorable transects. The results of this graphical analysis are summarized in several tables within this report. A similar graphical treatment was reported previously for the #K23 ground cloud measurements.[9]

These detailed analyses provide the data in a format that allowed direct comparison to model runs for specific times, altitudes, and distances from the release site. Preliminary comparisons documented significant differences between actual and predicted cloud behavior. The aircraft and imagery results are also available as comma-separated-variable files providing time, latitude, longitude, altitude, Geomet response, HCl concentration, and imagery-derived extent of the ground cloud. The intent of the MVP is to document the results in sufficient detail to validate dispersion models.

2. Analysis

The Volume 1 report provided a test overview and data summary. That earlier report also provided a detailed description of the analysis methods used both for the imagery and for the aircraft's HCl measurements. Therefore, it is only necessary to provide the reader a brief review in this report.

2.1 Linear Interpretation of Imagery

There are several approaches to analyzing imagery. The simplest approach is to assume that the X pixels (i.e., horizontal pixels) correspond to azimuth and the Y pixels (i.e., vertical pixels) correspond to elevation. This is an excellent assumption for an image recorded with the camera held horizontal or with a camera only slightly inclined while using a reasonably narrow field of view. The equations used in the linear interpretation of the imagery are:

$$dX \times \text{hdpp} = dAZ \qquad \text{where hdpp = horizontal degrees per X pixel}$$

$$dY \times \text{vdpp} = dEL \qquad \text{where vdpp = vertical degrees per Y pixel}$$

Using known landmarks, one can calculate the azimuth (AZ) and elevation (EL) from the imagery site to each landmark. Therefore, the "X,Y" pixel pair that corresponds to each known landmark is calibrated in terms of AZ and EL from the imagery site. If one has two landmarks in an image, one can calculate the dX and dY (i.e., number of pixels) that correspond to the dAZ and dEL (i.e., number of degrees) between the landmarks. Therefore, one can calculate the hdpp and vdpp (i.e., number of degrees per pixel) for the image for the horizontal and vertical axes. Knowing the total number of horizontal (640) and vertical (480) pixels in the image, one can calculate the horizontal and vertical field-of-view (FOV) of the image. Lastly, for any image that is calibrated (i.e., known landmark and known FOV), one can calculate the AZ and EL for any other pixel in the image using the "linear" correlation between dX and dY with dAZ and dEL, respectively.

The EL can then be used to calculate the height for an object at a known distance from the imagery site. Likewise, the angular size of an object (i.e., horizontal diameter in degrees azimuth and vertical diameter in degrees elevation) can be converted to physical dimensions if one knows the distance of the object from the imagery site.

Alternatively, when one sees the same object from two sites at the same time, one can calculate the closest approach (i.e., intersection) of the rays defined by the AZ and the EL of the object in the images at each site. The closest approach of such rays triangulates the altitude, latitude, and longitude of the object or feature. We have used this approach to triangulate the Titan IV ground cloud's position and extent by sequential analysis of pairs of imagery from multiple sites.

We recently documented[10] that the linear interpretation of imagery (used in this report) is accurate for low elevations (i.e., less than 20°) and for objects contained within reasonable fields of view (i.e., 20° to 30°). This was the case for the #K15 exhaust cloud imagery.

2.2 PLMTRACK Analysis of Imagery from Two Sites

Brian P. Kasper created and maintains the PLMTRACK program at The Aerospace Corporation. PLMTRACK provides a convenient way of triangulating the position of an object using imagery from two sites. PLMTRACK provided an absolute method of triangulating the position of the abort (or exhaust) cloud without making any assumptions regarding the position of the cloud. The analyst drew a box about the cloud in simultaneously acquired images from two sites. The edges of the box touch the top, left, right, and bottom extremes of the cloud as illustrated by Figure 1 (i.e., the shaded rectangle represents the image boundaries, while the ellipse represents an abort or exhaust cloud). PLMTRACK calculates the nearest approach for various rays, as illustrated by Figure 1 (i.e., as a ground projection of the cloud along with several rays from each camera site). The rays are defined by the middle of each of the edges of the boxes and the center of the boxes. These rays define the broadest extent and the position of the cloud in all observable dimensions as illustrated by the Cartesian plot of PLMTRACK results in Figure 2. In Figure 2, the site locations and rays are actual #K15 ground cloud data, while the outline of the cloud was synthesized for heuristic purposes.

The PLMTRACK analysis documented not only the Cartesian extent of the cloud, as illustrated in Figure 2, but also the x,y,z coordinates for the top, middle, and bottom of the cloud for each pair of images. Therefore, we will compare the imagery-derived maximum extent of the cloud to the extent derived by aircraft HCl sampling of the same exhaust cloud.

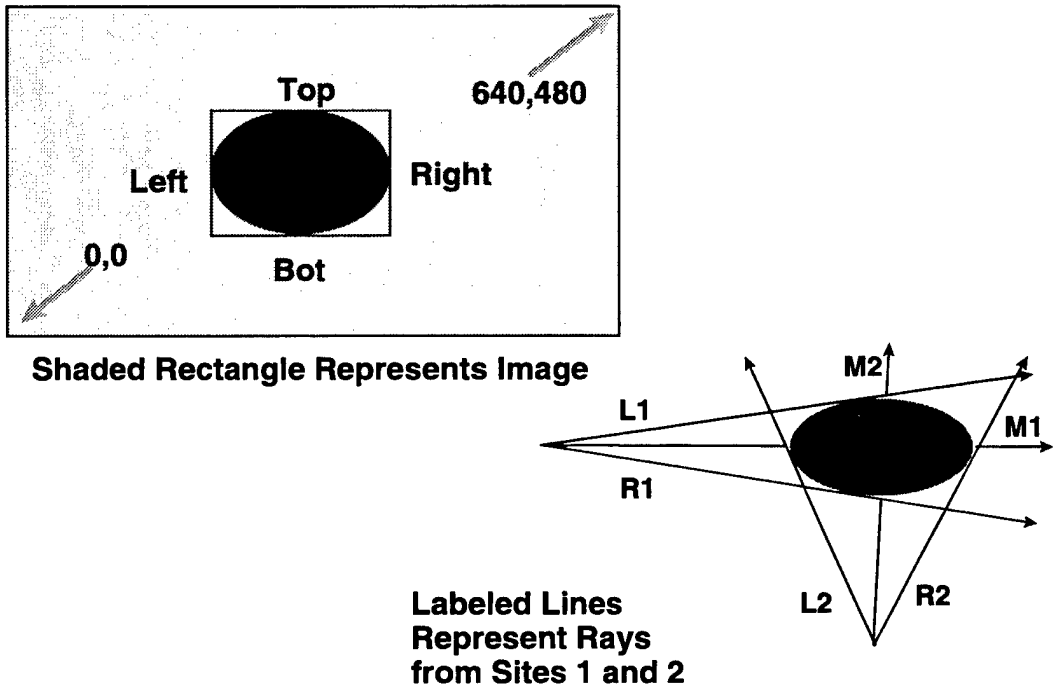

Figure 1. PLMTRACK box method within an image and projected onto ground plane.

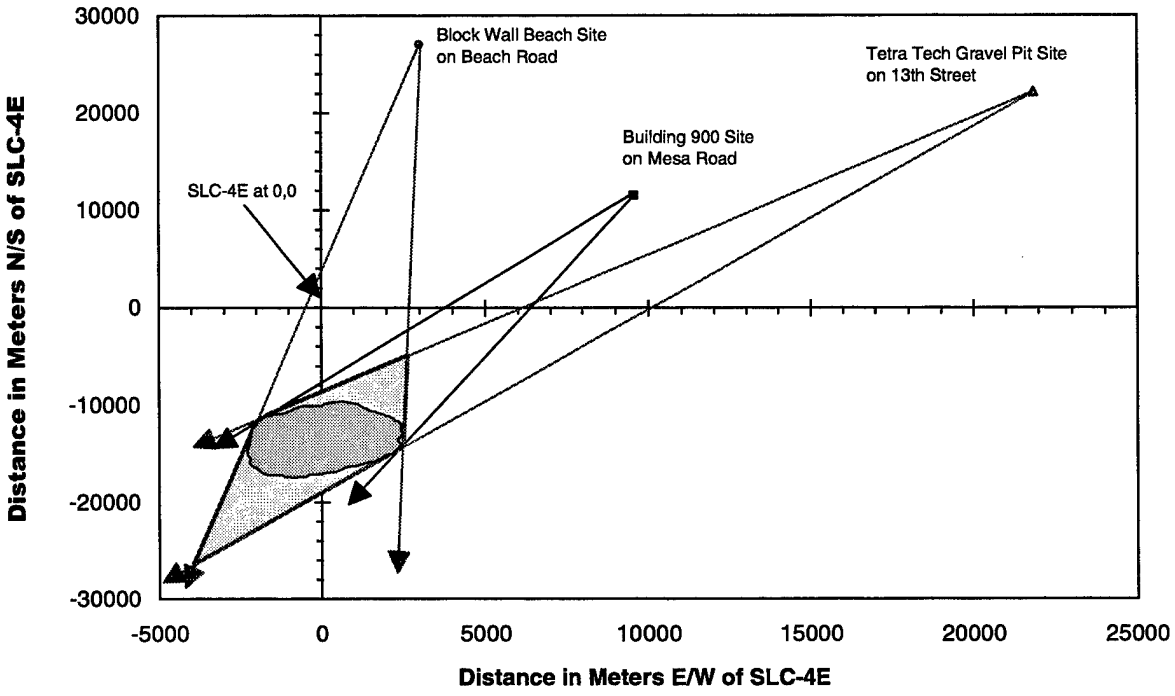

Figure 2. PLMTRACK ray tracing and extent of Titan IV #K15 exhaust cloud (T+8.0 min).

2.3 Geomet HCl Measurements

As described in detail in Chapter 5 of the test overview report,[4] I-NET, a NASA contractor, modified a Geomet for mounting in the nose of a Piper (PA-44-180) Seminole (a twin-engine, four-seat aircraft). The Geomet is a total HCl monitor that produces a response proportional to the combined HCl present in both the vapor or the aerosol phases. It reports the HCl concentration as parts-per-million (ppm) by volume (i.e., $V_{HCl}\ 10^6 / V_{total}$). This instrument sampled the air through a horizontal 4-ft long ceramic inlet wetted with a bromate/bromide-containing reagent. The HCl diffuses to the wetted walls of the ceramic tube and produces bromine vapor through reactions with the reagent. The bromine vapor is swept into a buffered hydrogen peroxide/Luminol solution, resulting in photoluminescence detected by a filtered photometric detector. I-NET disabled the Geomet's autoranging electronics so that a single range produced a millivolt response that was proportional to the combined HCl vapor and aerosol concentration entering the inlet. I-NET calibrated the Geomet against HCl vapor before and after the #K15 mission.

SRS Technologies Inc., a contractor, provided an interface between the I-NET laboratory and the Florida Institute of Technology (FIT) flight crew. NASA, NOAA/Air Resources Laboratory/Field Research Division, I-NET, SRS, and FIT cooperated in the integration of the NOAA data system, the FIT aircraft, and the Air Force Geomet into an airborne sampling and data logging system. FIT personnel piloted the aircraft during the #K15 mission, while 45th AMDS/SGPB personnel operated the NOAA data system and the Geomet detector. The NOAA data system logged GPS time and position as well as Geomet response every 0.25 s during the flight. NOAA provided a comma-separated-variable (csv) data file to the Aerospace Corporation.

As stated previously, the aircraft's altitude was measured using a global positioning system (GPS) receiver using regular service (no differential corrections were available for the VAFB area during this mission). The GPS altitude data were recorded as meters relative to mean sea level (MSL). Upon landing at the Santa Maria airport, the GPS altitude of the aircraft varied by 100 m over a 5-min period, ranging from 40 to 140 m. The actual runway height was 79 m (259 ft) MSL. Therefore, the GPS receiver appeared to function as expected while on the runway, delivering altitude data well within the regular GPS precision of ±250 m.

2.3.1 Reference for Altitudes

When comparing the aircraft's GPS-derived altitude (i.e., m MSL) to the imagery, rawinsonde, and REEDM data, it is essential to use the same frame of reference for measuring the height. REEDM reports the predicted height of the exhaust cloud relative to MSL and relative to ground level but incorrectly assumes that the height of the rawinsonde release site is the same as the height of the launch pad. This is the case for Cape Canaveral but is not the case for VAFB and results in a significant error in REEDM's output. We assert that REEDM's predicted height above ground level (AGL) was intended to be height above origin, which for a launch is height above the launch pad NOT above the rawinsonde release site. Therefore, in Chapter 2 of the test overview report,[4] the observed height of the imaged cloud and the predicted (i.e., by REEDM) height of the stabilized cloud were reported in meters above SLC-4E (i.e., above the launch pad). For this conversion, we assumed the height AGL reported by REEDM was the same as the height above SLC-4E. Since SLC-4E is 501 ft (153 m) above MSL, height relative to SLC-4E is converted to height MSL by adding 501 ft (153 m). Since REEDM incorrectly uses the height of the rawinsonde release site (368 ft, 112 m) rather than the height of the launch pad (501 ft, 153m) for its conversion of height AGL to height MSL, the height MSL reported by REEDM in Appendix A[4] is low by 41 m (133 ft).

2.3.2 Geomet Calibration Data

The Geomet's configuration was equivalent for the #K23, #K15, #K22, and #K16 missions. However, I-NET did not log the calibration response curves for the #K15 mission. Instead, for the #K15 calibrations, I-NET personnel merely noted the values of the plateau responses of the Geomet while being challenged against the calibration gas prior to the mission, subsequent to the mission with depleted reagent, and subsequent to the mission after recoating the inlet with reagent. For the #K15 mission, the plateau responses to the calibration vapor ranged from 0.92 V prior to launch, 0.585 V after launch (before recoating the inlet with reagent and with a –0.019 offset for zero air), and 0.662 V after recoating the inlet and rezeroing the detector. Therefore, the Geomet's plateau response to the calibration vapor degraded to 66% of its pre-flight value during the #K15 mission. Recoating the inlet with reagent recovered a few additional percentage points of the loss in response, yielding only 72% of the pre-flight value. This behavior is qualitatively consistent with the #K16 response curves included in the test overview report.[4]

The Geomet calibrations are HCl vapor challenges using constant concentration for long exposure times. Those data illustrated that the Geomet has an almost instantaneous response to sudden large changes in HCl vapor concentration but requires a longer time to reach the plateau response. Therefore, the Geomet should accurately map the extent, but not necessarily the strength of the Titan IV exhaust cloud.

2.3.3 Geomet Response Characteristics

The response characteristics of the Geomet detector are not perfectly matched to aircraft sampling. As configured for Titan IV missions (#K23, #K15, #K16, and #K22) and as illustrated by the #K16 data included in the previous report,[4] the Geomet requires more than 15 s to reach 90% of its plateau response as deployed for the Titan IV missions. In addition, the response time changes as a result of exposure to HCl vapor (i.e., the second exposures) were faster than the first exposures after coating the inlet. This is consistent with passivation of active sites within the freshly coated inlet. The magnitude of plateau response, as well as the time to reach it, can worsen when the exposure times are extremely long (as in the #K16 mission, which had an hour hold prior to extended sampling of the launch cloud). This is consistent with depletion of the reagent that coats the inlet. For all of the Titan IV missions, the Geomet's inlet was coated with reagent once prior to the flight. Therefore, one would expect some variation in response characteristics during each sampling mission. In spite of these difficulties, we believe the Geomet has some useful features that are discussed in the following paragraphs.

2.3.3.1 Accurate Integrated HCl Dose

The Geomet's raw response and its integrated response were plotted against time for the mission #K16 pre-flight and post-flight calibrations in the previous report.[4] Those plots documented that the Geomet accurately integrated the total HCl dose for HCl vapor exposures. There was quantitative behavior (i.e., more than 98% of total dose) for the pre-flight calibration and over 92% of total dose for the post-flight calibrations. Since the Geomet was configured similarly for all of the Titan IV missions, the #K16 response data provide an interesting complement to the less detailed calibration data available for the #K15 mission. Since the Geomet provides accurate total HCl dose for each pass through the cloud, one can calculate the average HCl concentration using the time of the exposure and the total dose. The following paragraphs discuss cloud edge detection by the Geomet. Accurate edge detection is the same as accurate exposure time measurement.

2.3.3.2 Accurate Edge Detection and Peak Location Reporting

Since the aircraft is moving at more than 70 m/s, and it takes 15 s (or more) for the Geomet to provide 90% response to the new HCl concentration, it is likely that the Geomet may underestimate the maximum HCl concentration for short encounters with the cloud. However, the initial response to 10% of the plateau response is extremely rapid. Thus, there should be little offset between the Geomet's first indication of change and the aircraft's encounter with the edge of the exhaust cloud or the maximum concentration within the exhaust cloud.

The temporal, relative, and absolute accuracy of the Geomet's response to the Titan IV #K15 exhaust cloud was documented for the first few minutes after launch by comparison of the Geomet's cloud data to that of the Spectral Sciences gas filter correlation (GFC) spectrometer that flew on the same aircraft for the #K15 mission. The GFC spectrometer provided an instantaneous response to the exhaust cloud and was mounted beneath the aircraft. The inlet to the Geomet extended out of the front of the same aircraft.

The data from the GFC data were compared[4] to the Geomet data to establish the significance of the Geomet's response characteristics for actual aircraft sampling of Titan IV #K15 exhaust cloud. The

HCl concentration profile was derived in three ways for a single cloud pass: (1) Geomet response, (2) 3.85 s averaging of the GFC data, and (3) 18 s averaging of the GFC data. Careful comparison of these data revealed no shift in time between the maximum concentration reported by the 3.85 s GFC spectrometer data and the maximum reported by the Geomet detector. A 6–12 s shift in time would have corresponded to a 0.5–1 km shift in position for the maximum of the cloud based upon a 70 m/s aircraft speed. The width (i.e., onset of rise and start of fall) is identical for the Geomet and for the 3.85 s GFC spectrometer data. This is consistent with good edge detection by both detectors. Comparison of the 18 s GFC data to the Geomet data documented the same value for the maximum HCl concentration but not the same temporal (i.e., positional) mapping of the cloud. Therefore, those data were consistent with the Geomet's documented two-part response curve: (1) rapid initial response to a large change in HCl concentration and (2) a slow rollover in response prior to reaching a plateau. Since the Geomet has both fast and slow components of response, it appears that the Geomet is able to accurately map the extent and shape of the exhaust cloud by virtue of its fast response to large changes in concentration. The tail on the Geomet peaks was consistent with the tail (i.e., slow recovery to baseline) observed during challenges against calibration vapors.

Since the GFC technique only responds to vapor while the Geomet responds to total HCl (aerosol and vapor), this treatment cannot provide quantitative rise characteristics for the Geomet. In addition, the noisy GFC data may overestimate the integrated HCl (i.e., bigger area than Geomet). However, one can conclude, qualitatively, that the Geomet not only provides integrated HCl for each pass through the cloud but also maps the extent and position of the cloud by virtue of the fast component of its complicated response function. Therefore, one can calculate the average HCl concentration for each pass through the cloud from the accurate extent (i.e., time in the cloud) and the accurate total HCl dose (i.e., ppm-s).

3. Results

The results of the quantitative analysis of the ground cloud imagery were documented in a previous report[4] as were the results from the Geomet and Gas Filter Correlation Spectrometer (GFC) sampling of the HCl within the ground cloud. This report extends the analyses in three ways: (1) correlation between the aircraft Geomet's HCl concentration profiles and the imagery-derived maximum extent of the ground cloud, (2) graphical reporting of the aircraft Geomet's HCl data with greater spatial and temporal resolution than was possible in the data summary report, and (3) comparison of the measured cloud characteristics to REEDM predictions. Simultaneous imagery and aircraft sampling data are available for the first 11 min after launch and are compared in the first portion of the results. The second portion of the results discusses the standardized series of plots included as separate appendices for each 10 min of the aircraft's sampling. The third portion of the results analyses the trends and compares them to REEDM predictions. This method of reporting the aircraft's HCl results allows direct graphical comparison with dispersion model output.

3.1 Comparison of Aircraft HCl Profiles to Imaged Ground Cloud Extent

The first six aircraft encounters with the exhaust cloud (i.e., passes through the cloud) occurred between 3 and 10.2 min after launch. During this same period, the quantitative imagery documented the extent of the exhaust cloud using both visible and IR imagery. This section provides Cartesian plots that overlap the aircraft Geomet's HCl sampling data and imagery-derived extent of the exhaust cloud. These data illustrate consistent edge detection by the aircraft and by the quantitative imagery. In addition, a second series of plots document the instantaneous HCl concentrations, the average HCl concentrations, the total HCl dose (i.e., in ppm-s), and the time in the exhaust cloud for each of these first six aircraft encounters with the exhaust cloud. For completeness, this section also provides an altitude plot for the imagery-derived extent of the cloud and for the aircraft Geomet's HCl concentration data. Therefore, this section provides an imagery-derived three-dimensional extent for the ground cloud as well as aircraft-derived (i.e., Geomet) HCl concentration profiles within well-identified regions of the ground cloud.

3.1.1 Cartesian Extent of the Ground Cloud for Passes 1–6

Figure 3 documents aircraft-derived and imagery-derived exhaust cloud data collected between 3 and 10.2 min after launch. In Figure 3, the aircraft's Cartesian position is labeled with HCl concentrations. For comparison, Figure 3 includes selected imagery-derived polygons that document the maximum extent of the exhaust cloud over a similar period. Figure 3 reveals that the center of the exhaust cloud is mapped identically both by the aircraft's Geomet HCl monitor and by the quantitative imagery. Likewise, both methods document movement of the cloud in a southerly direction between 4 and 10 min after launch.

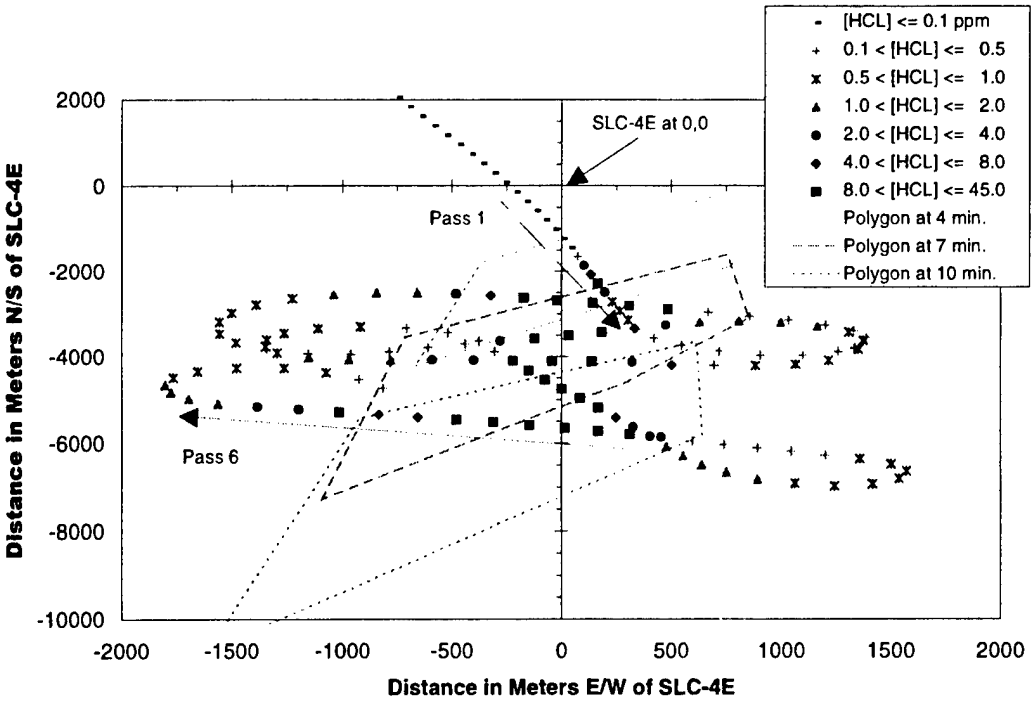

Figure 3. Imagery- and aircraft-derived Cartesian cloud extent (T=3-10.2 min).

Figures 4 through 9 document individual Cartesian plots for each of the six passes shown in Figure 3. In each case, the leading edge of the exhaust cloud reported by the aircraft's Geomet detector is consistent with the edge of the imagery-derived maximum extent (i.e., polygon) of the exhaust cloud. By consistent, the Geomet should not report significant HCl concentration outside of the imagery-derived polygon. As documented in the prior #K15 report,[4] the Geomet detector provides a fast initial indication of exposure but is slow to recover (i.e., has a long tail in its recovery curve). Therefore, it is expected that the aircraft will continue to report decreasing HCl concentrations after it has already exited the exhaust cloud. Review of Figures 4 through 9 confirms that the slow recovery produces decreasing HCl concentrations (i.e., an artifact) that extend beyond the imagery-derived polygon only on the tailing leg of each aircraft encounter with the exhaust cloud. However, in spite of this long tail, the aircraft's HCl measurements do map the tailing edge of the exhaust cloud as the last high-level hit preceding the Geomet's slow recovery (i.e., decreasing HCl concentrations after the encounter). Review of Figures 4 through 9 reveals a fairly consistent detection of the tailing edge of the exhaust cloud by using the last strong HCl hit (i.e., HCl > 2 ppm for passes 1 through 5) from the aircraft and the edge of the imagery-derived polygon. One must remember that the polygon represents the maximum observable extent (i.e., the analyst's choice) at all altitudes while the aircraft sampled the cloud at one altitude for each encounter. For pass 6, the Geomet's tailing edge of the cloud extends slightly beyond what the analyst defined as the ground cloud in the imagery. However, the Geomet's extended tail is due, in part, to a spike in HCl concentration (i.e., concentrated eddy) that occurred as the aircraft was leaving the imagery-derived extent of the cloud. This relatively small, concentrated, and detached puff of the cloud was possibly ignored (or missed) by the analyst when viewing the imagery. This is a reasonable assumption since the signal- to-noise ratio

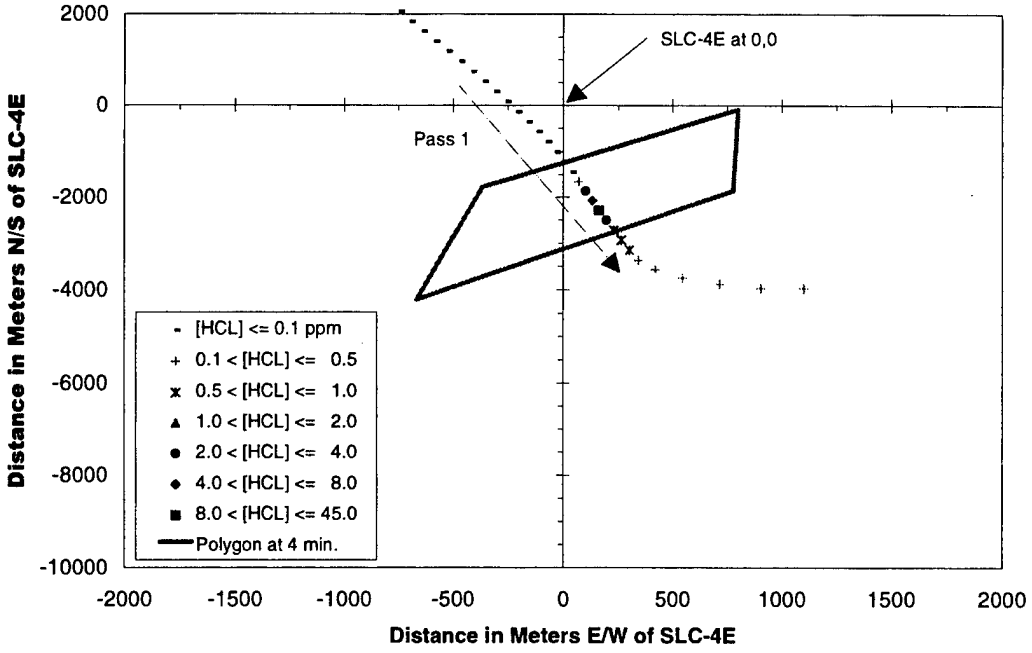

Figure 4. Pass 1 (T=3.0-4.5 min) versus imagery-derived polygon (T=4 min).

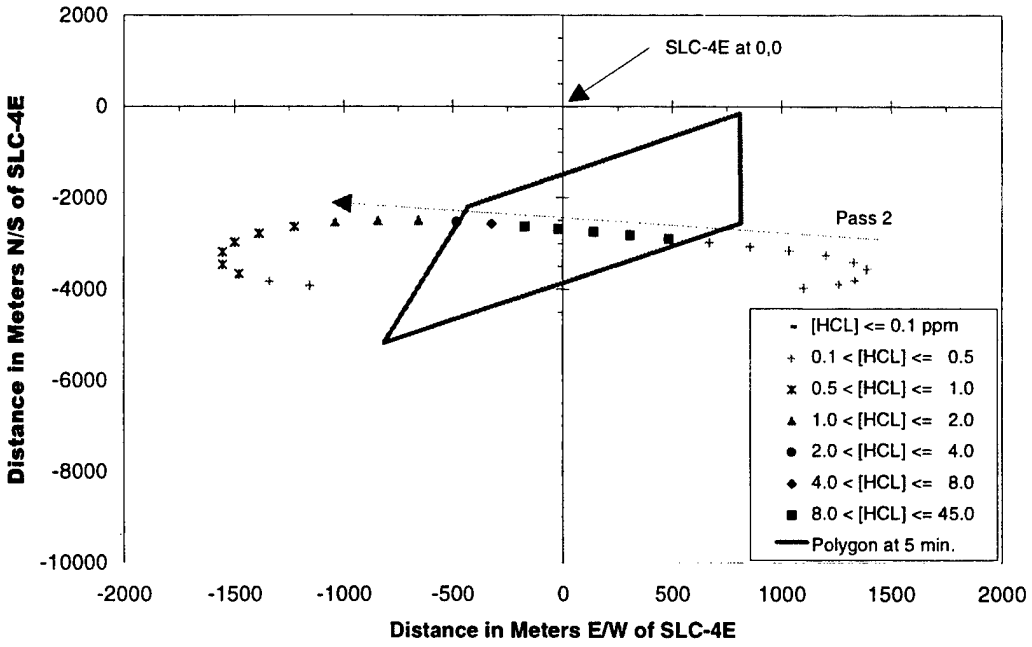

Figure 5. Pass 2 (T=4.5-5.8 min) versus imagery-derived polygon (T=5 min).

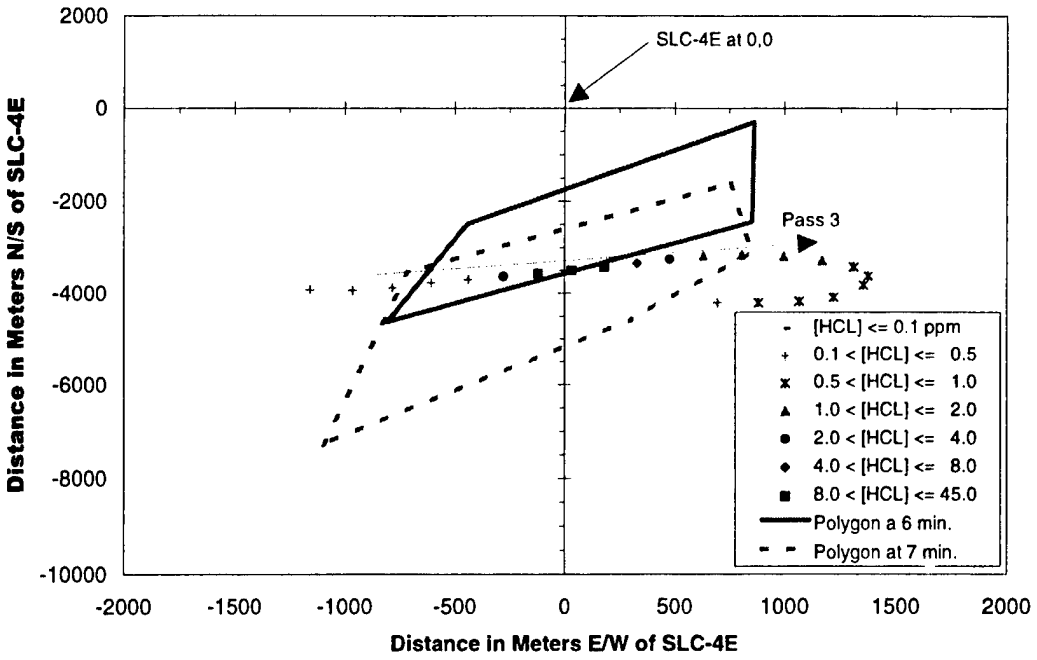

Figure 6. Pass 3 (T=5.8-6.85 min) versus imagery-derived polygons (T=6 and 7 min).

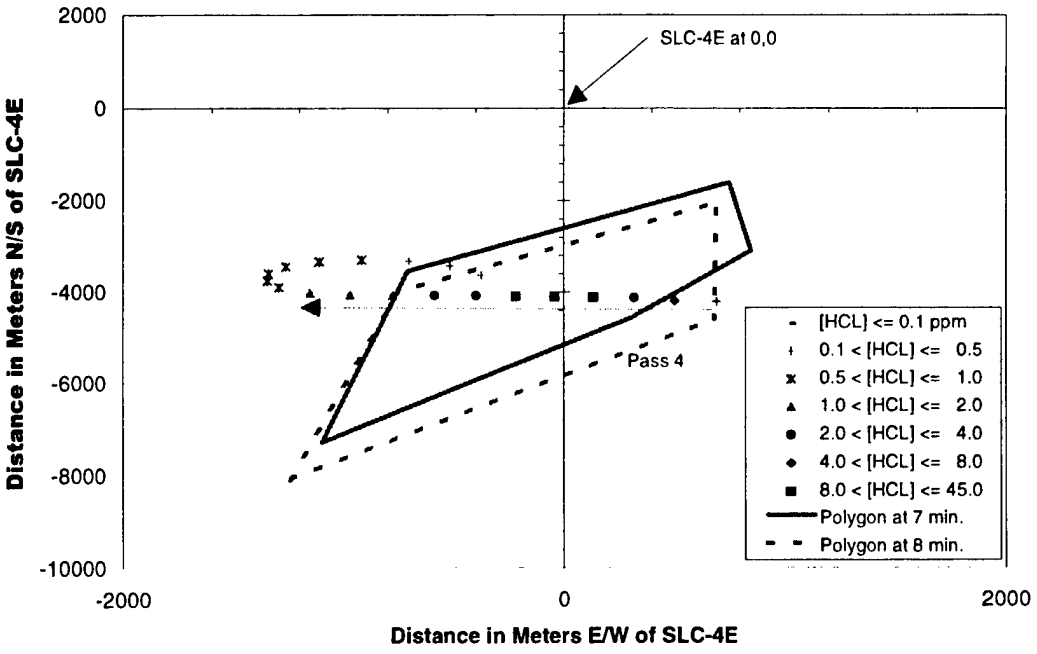

Figure 7. Pass 4 (T=6.85-7.8 min) versus imagery-derived polygons (T=7 and 8 min).

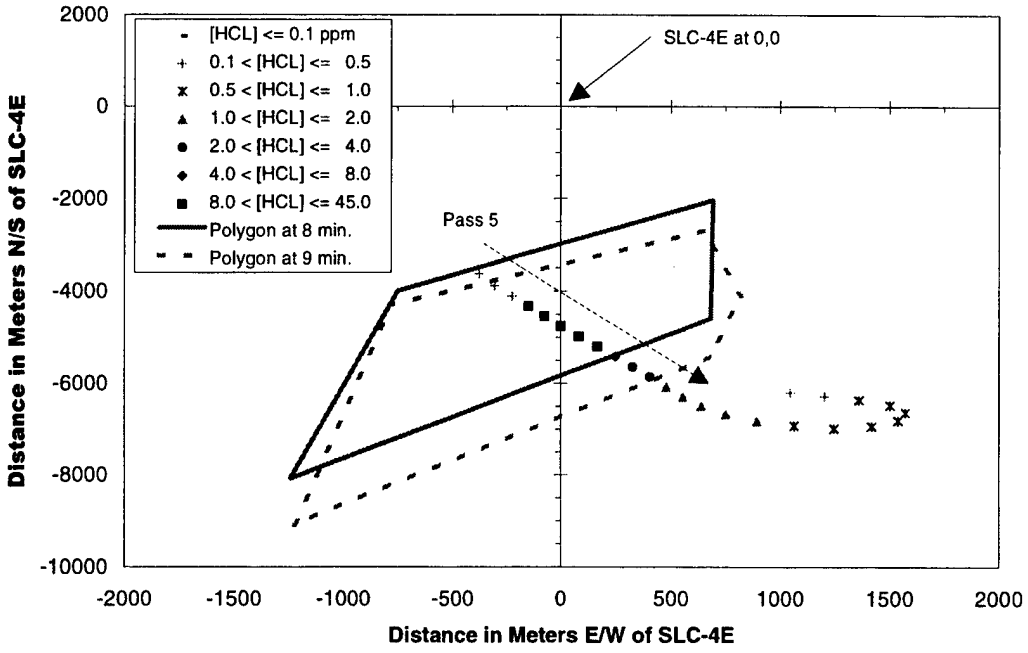

Figure 8. Pass 5 (T=7.8-9.05 min) versus imagery-derived polygons (T=8 and 9 min).

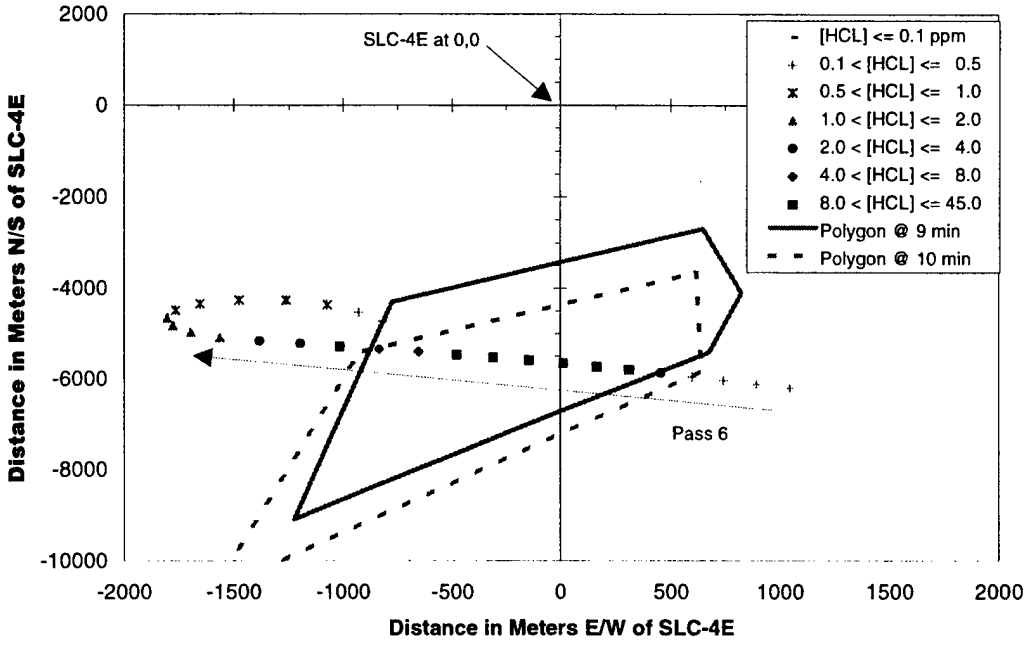

Figure 9. Pass 6 (T=9.0-10.2 min) versus imagery-derived polygons (T=9 and 10 min).

was decreasing with time for the imagery, and pass 6 was the last aircraft encounter that was compared to the imagery. The 2 ppm threshold corresponds to 5 to 6% of the maximum HCl reported in the first 6 passes. Therefore, the bulk of the cloud is contained in the imagery-derived polygons.

Figures 10 and 11 are visible and IR exhaust cloud images that reveal the magnitude of the variation in cloud extent and density as viewed from building 900 site at T+3.0 min after launch. Based upon

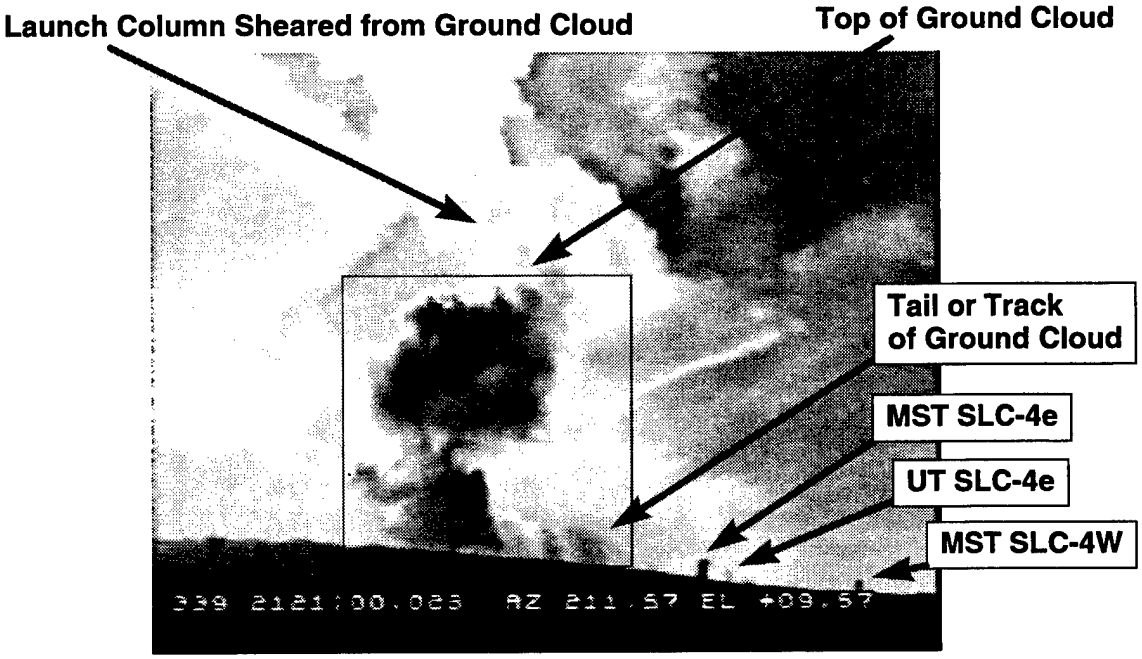

Figure 10. Visible image of ground cloud (T+3.0 min) from building 900 site.

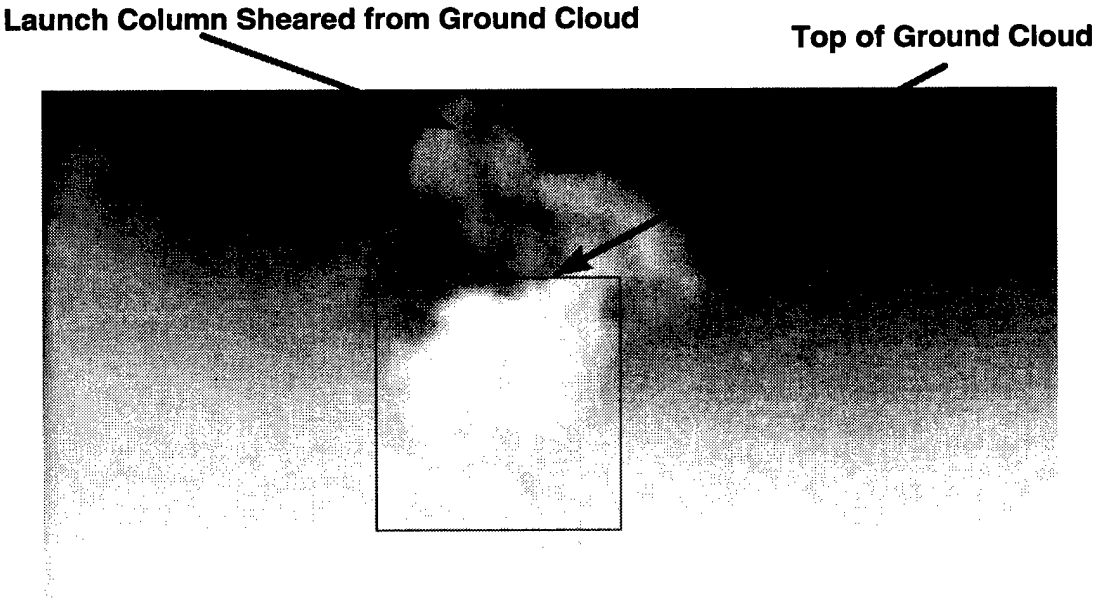

Figure 11. Infrared image of the ground cloud (T+3.0 min) from building 900 site.

review of Figures 10 and 11, the imagery-derived maximum extent of the ground cloud (i.e., for all altitudes) will probably be greater than the extent sampled by any aircraft encounter (i.e., at a single altitude). This is consistent with the fact that the extent mapped by the imagery-derived polygons (i.e., Figures 4–9) was larger than the extent of the highest HCl concentration hits (i.e., extent of the cloud by the Geomet detector) for almost every aircraft encounter. As mentioned previously, the agreement was reasonable even for pass 6, which occurred when the signal-to-noise ratio was poorest for the imagery. The complicated cloud structure shown in Figures 10 and 11 are also consistent with the large fluctuations in HCl concentration within the cloud. As shown previously,[4] and in a later section of this report, the Geomet detector documents large fluctuations in the HCl concentration during each aircraft encounter with the exhaust cloud.

It is apparent from review of Figures 10 and 11 that the visible and IR exhaust cloud images have dramatically different contrasts for cloud details. The visible imagery documents ground-level structures even against the hillside. These same structures are difficult or impossible to see in the IR since they are at (or nearly at) the temperature of their surroundings or their background. The infrared sees a large radiance from the atmosphere at the horizon. The radiance decreases rapidly with elevation since the integrated atmosphere within line-of-site decreases rapidly with elevation. It is apparent that the IR imagery more easily detects the top of the cloud and the launch column against the cooler high-altitude clouds than the bottom of the cloud against the humid atmospheric background. In contrast, the visible imagery is complicated by scattering of sunlight from high-altitude atmospheric clouds. Therefore, the visible and IR imagery provide complimentary data.

3.1.2 Average HCl Concentration and Total HCl Dosage for Passes 1–6

The analysis section documented two useful properties of the aircraft's Geomet HCl detector: (1) accurate mapping of the edge of the exhaust cloud (and the position of maximum concentration) and (2) quantitative reporting of the total HCl dosage. In the previous section, Figures 3 through 9 supported the claim that the Geomet accurately detects the edge of the cloud by comparing the aircraft's Geomet HCl data to the imagery-derived maximum extent of the exhaust cloud. In regards to total HCl dosage, Figures 12 through 17 plot the aircraft Geomet detector's HCl concentration data against time for each of the first six passes through the #K15 exhaust cloud. In addition to plotting the instantaneous HCl concentration, each plot is labeled with the average HCl concentration, an error estimate for the average concentration, the total HCl dosage encountered in that pass, and the time spent within the exhaust cloud. The horizontal line in these figures documents the average HCl concentration by its height and the time spent in the cloud by its length.

The error estimate for average HCl concentration is expressed as a percentage of the maximum average concentration. For each aircraft encounter with the exhaust cloud, the maximum average concentration is calculated by dividing the total HCl dose by the time spent in cloud. One must remember that the Geomet may not accurately report the instantaneous concentration but it does accurately report the total dose and the extent of the cloud (i.e., time spent in the cloud).

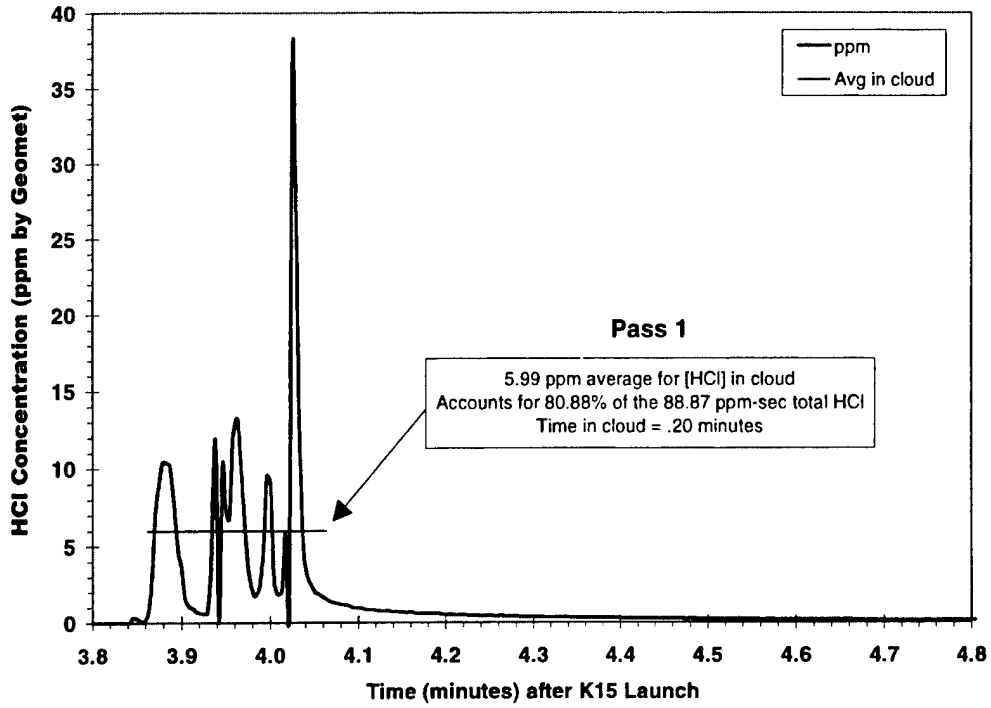

Figure 12. Pass 1 (T=3.0-4.5 min) HCl concentration and dosage data.

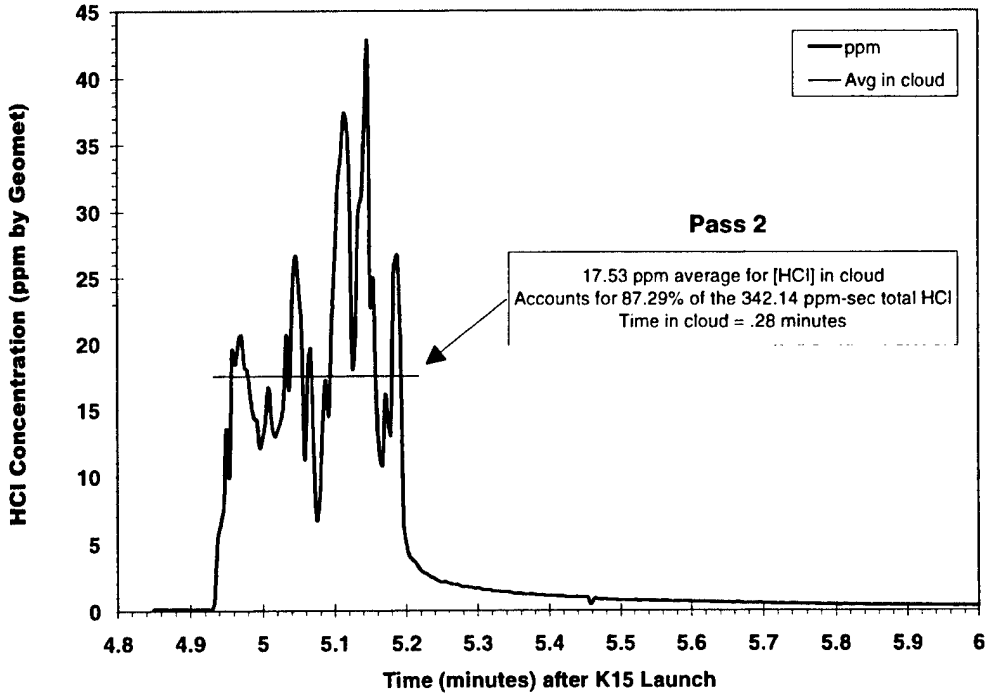

Figure 13. Pass 2 (T=4.5-5.8 min) HCl concentration and dosage data.

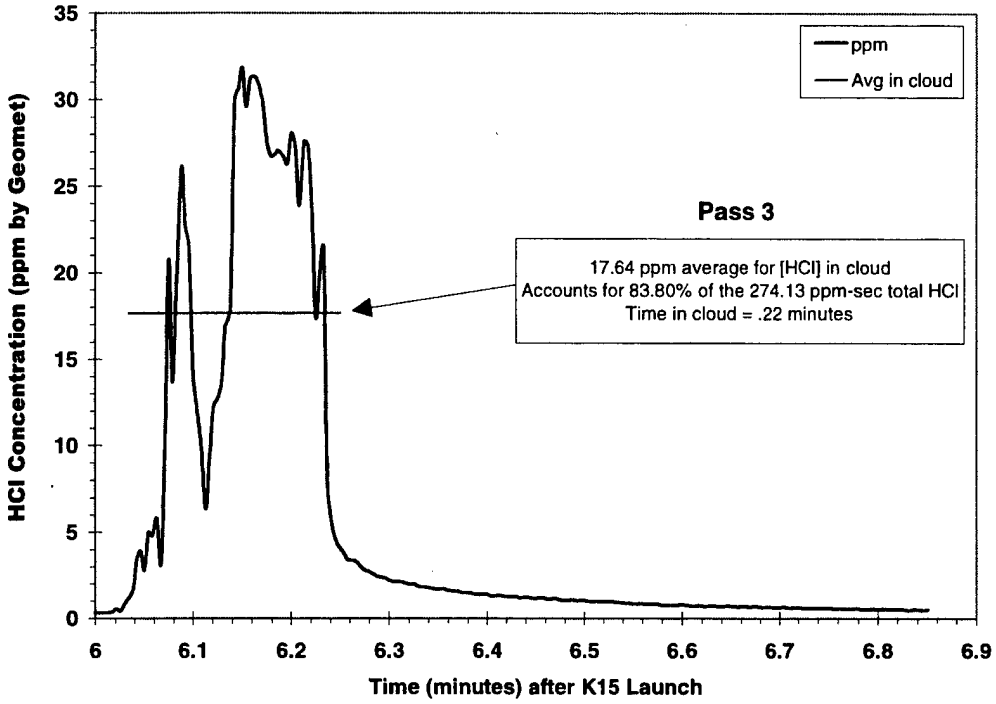

Figure 14. Pass 3 (T=5.8-6.85 min) HCl concentration and dosage data.

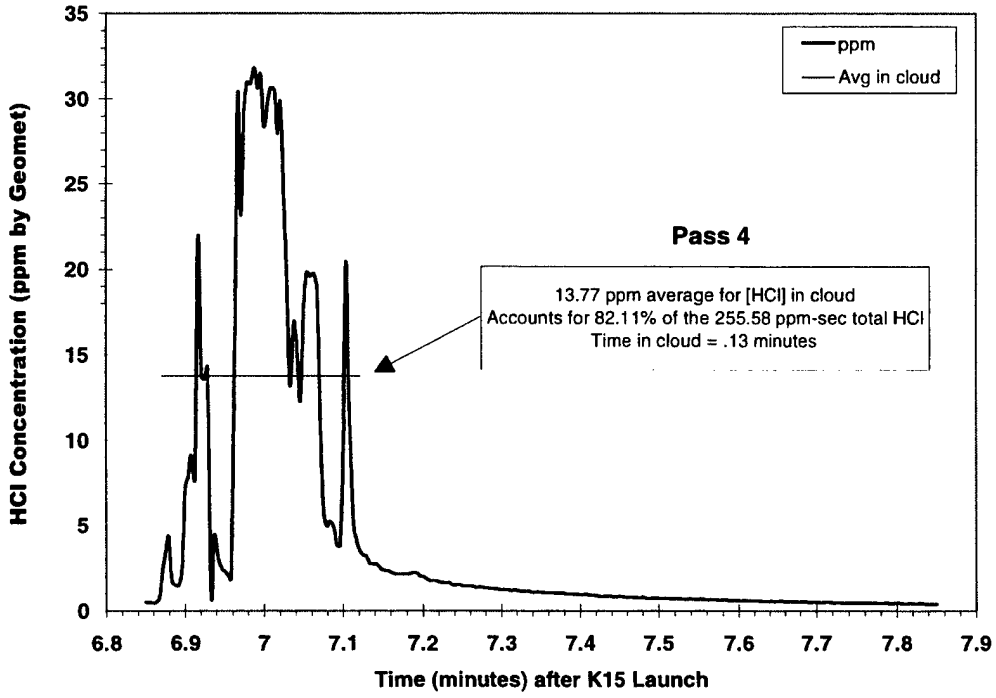

Figure 15. Pass 4 (T=6.85-7.8 min) HCl concentration and dosage data.

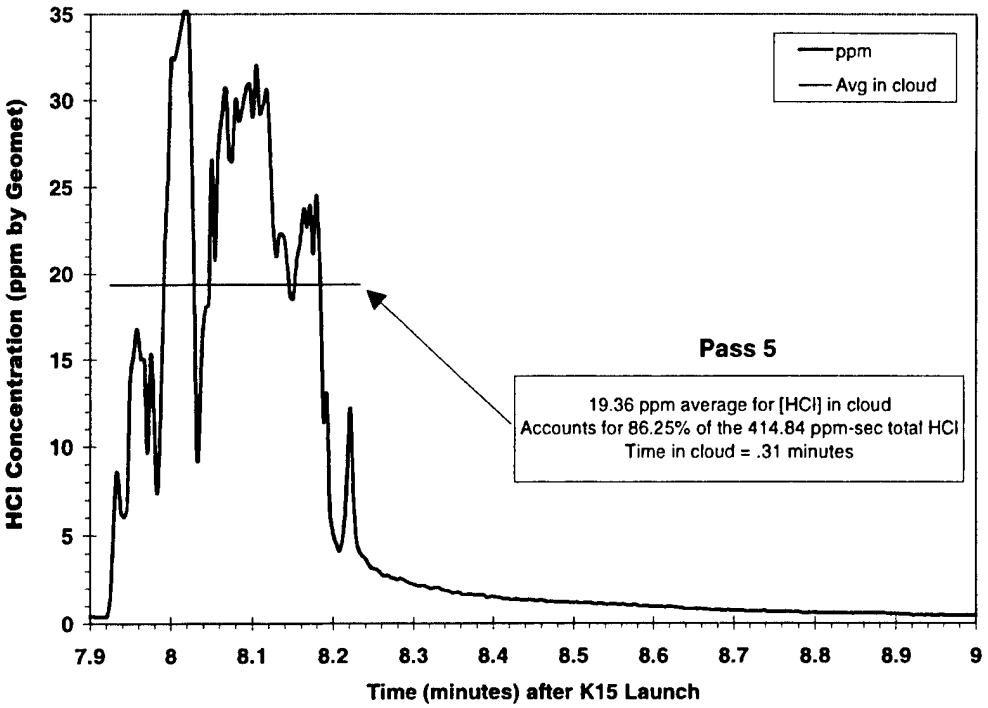

Figure 16. Pass 5 (T=7.8-9.05 min) HCl concentration and dosage data.

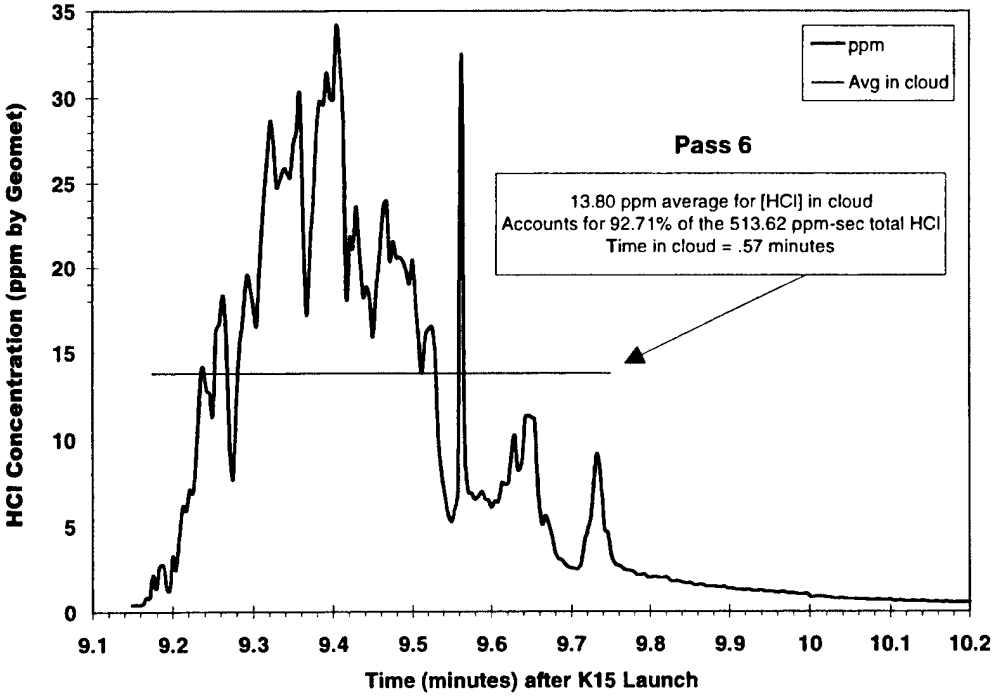

Figure 17. Pass 6 (T=9.0-10.2 min) HCl concentration and dosage data.

The difference between the maximum average HCl concentration and the measured average HCl concentration accounts for the fact that rapid changes in HCl concentration are smoothed by the Geomet's complicated response function (i.e., 4 s initial response versus 18 s plateau response). The magnitude of the difference is testimony to the fact that the Geomet's response function cannot follow rapid HCl concentration fluctuations within the cloud. The average concentration is only 81% of the maximum average concentration for the first pass (i.e., Figure 12) but is 93% of the maximum average concentration for the sixth pass (i.e., Figure 17). The results from these two encounters might be interpreted, incorrectly, as a decrease in the initially strong concentration gradients as the cloud mixes. However, review of the data from all six aircraft passes (i.e., Figures 12 through 17) reveals considerable variation not only in the complexity of the cloud's structure but also in the concentration gradients associated with eddy structures. Based upon these dramatic (and apparently discontinuous) differences between the first six aircraft encounters with the exhaust cloud, one must conclude that the aircraft's sampling pattern (i.e., what part of the cloud was sampled) complicates the interpretation of these data as a simple dispersion process. Indeed, pass 1 was a downwind pass that only sampled the eastern edge of the cloud (i.e., resulting in dramatic HCl concentration fluctuations) while pass 6 was a crosswind pass that sampled closer to the middle of the cloud (i.e., a more Gaussian HCl profile). In a later section, the data are filtered to allow comparison with REEDM predictions. Those discussions will document that the aircraft did not map the fullest extent of the cloud but did measure higher-than-predicted HCl concentrations.

So far, we have the maximum average concentration within the cloud and the horizontal extent for each of the first six passes through the exhaust cloud. In the next section, we provide the vertical extent and, thereby, complete our 3-D picture of the exhaust cloud.

3.1.3 Aircraft Altitude and Imagery-Derived Vertical Extent for Passes 1-6

The previous sections documented the Cartesian extent, the maximum average concentration, the total HCl dose, and the time spent in the exhaust cloud for each of the first six aircraft encounters with the exhaust cloud. Comparison of the aircraft's Cartesian extent with the imagery-derived maximum extent revealed that the aircraft flew through the middle of the imagery-derived horizontal extent of the ground cloud. Figure 18 documents the aircraft's altitude during each of the first six aircraft encounters relative to the imagery-derived vertical extent (i.e., altitude of the top and bottom) of the ground cloud. It is apparent from this figure that the aircraft sampled at approximately the same altitude for the first five passes and dropped in altitude for the sixth pass. As discussed in the previous section of this report and in the previous data report,[4] the signal-to-noise ratio for the imagery decreased as the cloud moved away from the imagery sites and dispersed. Therefore, the apparent increase in altitude for the bottom of the cloud after 5 min is probably an artifact caused by poor signal-to-noise for detecting the bottom of the cloud by imagery. In spite of this difficulty, all of the aircraft encounters are within the imagery-defined vertical extent of the ground cloud. Upon review of Figure 10, one can conclude that the first five passes went through the upper and larger lobe of the ground cloud. It is likely that the sixth pass also sampled the upper portion of the ground cloud. This assumption is based upon the extent of the sixth hit (i.e., almost a minute in duration); therefore, the aircraft was still within a wider portion of the cloud.

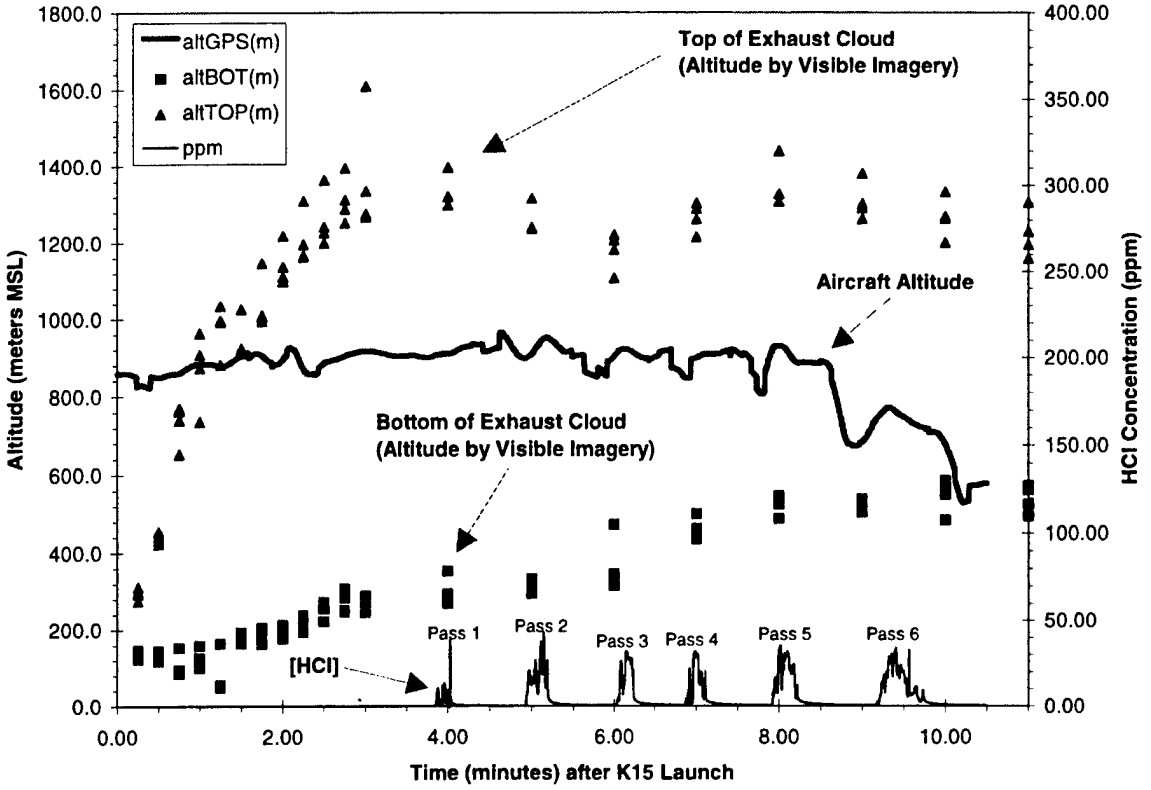

Figure 18. Altitude plot for aircraft and exhaust cloud (T = 0 to 11 min).

This portion of the results completes the 3D picture of the ground cloud for the first 11 min after launch. The 3-D picture includes not only the horizontal and vertical extent of the cloud but also the maximum average concentration for each aircraft transit through the middle portion of the cloud. At times greater than 11 min, the aircraft is the only source of cloud data. The next portion of the results provides a detailed graphical review of all of the aircraft data in 10-min time windows. Review of those plots allowed a compilation of data characteristic of each of the 41 aircraft transits through the ground cloud.

3.2 Detailed Plots of Aircraft-Derived HCl Profiles (10-min Intervals)

The previous section of the results provided a 3-D picture of the ground cloud based upon the combination of quantitative imagery of the entire exhaust cloud and aircraft transits through portions of the exhaust cloud. The imagery-derived extent of the cloud provided an outline of the cloud and allowed the interpretation of the aircraft's Geomet-derived HCl concentrations as transits through the middle portion of the ground cloud. There is no quantitative imagery for times longer than 11 min, but the aircraft sampled the ground cloud for 100 min. Therefore, one needs to analyze the aircraft data to determine its utility for mapping of the ground cloud trajectory and extent without complimentary imagery.

This portion of the results provides a detailed review of the aircraft data and describes the graphical methods applied to the data. Appendix B contains two plots for each 10 min of aircraft data (i.e., 0–10, 10–20, through 90–100 min). The two plots provided for each 10 min of flight are:

(1) A time plot documenting the aircraft altitude and the strength of the Geomet's HCl measurements (also, when available, the imagery-derived altitudes for the top and bottom of the ground cloud), and

(2) A Cartesian plot documenting the location and the strength of the Geomet's HCl measurements.

Table 1 refers to the data plotted in Appendix B and provides data characteristic of each aircraft transit through the ground cloud. Table 2 documents the aircraft-derived extent of the ground cloud based upon the start and end of HCl hits for each transit. Table 3 includes some of the cloud data from Table 1 and Table 2 and adds sampling information useful for interpretation of the significance of the data.

All three tables list the transit number (i.e., pass number) in the first column. Table 1 provides several characteristics for the maximum HCl hit for each pass including: the time (column 2), the peak HCl concentration (column 3), the sampling altitude (column 4), and the aircraft's polar location (i.e., distance in column 6 and angle in column 7). Table 1 also lists the plume-to-pad distance (column 8) calculated using the time (column 2) and the imagery-derived cloud speed (i.e., 9.2 m/s). Comparison of the column 8 distance to the column 6 distance reveals that the aircraft flew near the middle of the cloud for the first 6 passes (i.e., column 8 – column 6). This was shown to be true in the previous section of the results where the imagery-derived extent was compared to the aircraft's flight data. Table 1 provides a qualitative description of the type of pass in column 5 and a rough estimate of the polar extent of the cloud (i.e., the difference in distance in column 9 and the difference in angle in column 10 between the first and last hit for each transit). Table 2 provides the start and end times (columns 2 and 3), the start and end distances (columns 4 and 5), and the start and end angles (columns 6 and 7) for each aircraft transit through the exhaust cloud. The distances and angles define the polar position of the start and end for each transit relative to SLC-4E. Table 2 also documents the length (column 8) and bearing (column 9) for each transit. The length is the linear distance between the start and end of the transit, while the bearing is the angle between the start and end of the transit. The angle is used to determine the type of pass reported in Tables 1 and 3.

The aircraft's bearing is reported in rawinsonde convention for comparison to wind angles. An angle of 360° indicates an aircraft bearing to the South (i.e., with a wind from the North). An angle of 90° indicates an aircraft bearing to the West (i.e., with a wind from the East and perpendicular to a wind from the North). Since the exhaust cloud moved to the South (i.e., a wind from the North), aircraft bearings (i.e., Table 2, column 9) between 330° and 30° (i.e., 360° ±30°) are downwind passes (i.e., Table 1, column 5, "Type of Pass"). Likewise, aircraft bearings between 150° and 210° (i.e., 180° ±30°) are upwind passes. Crosswind passes include angles near 90° or 270° (i.e., within 30°). The analyst selected the start of a pass as the first Geomet response above baseline and the end of the pass with some bias (i.e., the end of the fast fall, therefore ignoring the slow recovery tail). Thus, the start and end are intended to be the edges of the cloud. The analyst did not correct for any lag time for the start of response or the start of fall. It is reasonable to assume that the lag time is symmetrical

(i.e., the same for the start and fall). Therefore, the length of the pass (i.e., the extent of the cloud) should be reasonably accurate. The lag time is probably a 1 or 2 s and was not measured by INET.

It is important to understand that the start and end of the pass are intended to map the main portion of the cloud and not the slow recovery of the Geomet after leaving the cloud. Therefore, the analyst used some bias in picking the start and end to accurately map the direction of travel and the extent of the cloud. For example, if the bulk of the hit was along a straight course, but the aircraft started its turn before the "tail" (i.e., the Geomet recovery curve) had reached baseline, the analyst picked the end of the sharp fall in concentration rather than some other point along the asymptotic approach to baseline. In most cases, the analyst was convinced that the start and end correctly mapped not only the extent but also the direction of travel since the aircraft typically flew out of the cloud before initiating its turn.

This was not the case for passes 16, 18, 19, 32, 34, 35, and 39, where the aircraft started its turn before there was a sharp drop in concentration (16, 34, 35, and 39), or the analyst marked only a portion of the sampled cloud (18, 19, and 32). The analyst chose the farthest extent and noted a "Partial Cross" as the type for pass 16. The analyst included the complete pass for passes 34, 35, and 39 but noted a "Partial/Curve" to indicate that the length and direction between the start and end do not represent the length and direction of the aircraft's encounter. Passes 18 and 19 are actually the eastern extreme and the western extreme portions of the cloud measured by one long straight aircraft transit and are separated by a parcel of air (i.e., are baseline resolved). Pass 27 is a similar encounter; however, it documents a bimodal distribution with more concentrated eastern and southern portions of the cloud as well as continuous HCl concentration between these pockets of HCl. Pass 32 quantifies a more concentrated pocket of HCl surrounded by a much more dilute and extended cloud. Except for passes 16 and 18, the aircraft maintained relatively constant altitude throughout each encounter with the exhaust cloud. The aircraft descended rapidly during pass 16 and ascended rapidly during pass 18. All encounters are fully documented by the graphical plots included in the appendices and by the parametric listings in the Tables 1 through 3.

The first five columns in Table 3 are identical to those of Table 1. The "Cloud Encounter" data included in columns 6 and 7 of Table 3 are identical to columns 8 and 9 of Table 2. The next three columns in Table 3 document the apparent cloud speed needed to reach the position of the maximum hit at the time of the maximum hit. The cloud speed is reported as a vector (i.e., column 8) and its components (i.e., N/S velocity in column 9 and E/W velocity in column 10). The average cloud speed from column 8 is 10.29 m/s, with a standard deviation of 0.48 m/s. These values are used to filter the data for hits that are close to the center of the cloud. The use of this average assumes that the pilot attempted to fly through the center of the cloud on the average. Finally, the last column in Table 3 categorizes the data as to the portion of the cloud that was sampled (i.e., due south, westerly, easterly, or very easterly). The E/W component of the cloud speed to maximum hit was used to define these as follows: W has more negative E/W speed than –0.45 m/s; S has an E/W speed between –0.45 and +0.45 m/s; VE has more positive E/W speed than +1.0 m/s; and E has an E/W speed between +0.45 and +1.00 m/s.

Table 1. Summary of Aircraft Sampling Data for the #K15 Ground Cloud

No.	Time of Pass at max. (min)	Peak HCl at max. (ppm)	Sampling Altitude at max. (meters)	Type of Pass[1]	Aircraft Location w.r.t. SLC-4E at max. Δ(m)	θ(°)	Plume to Pad[2] (μ)	Plume Parameters ΔD (m)	Δθ (°)
1	4.03	37.2	910	Downwind	2364	355.79	2225	994	2.35
2	5.15	42.2	949	Crosswind	2647	2.64	2843	387	20.17
3	6.15	31.8	922	Crosswind	3499	359.47	3395	381	13.36
4	7.00	31.8	898	Crosswind	4121	357.27	3864	148	13.28
5	8.02	35.3	930	Downwind	4609	0.62	4427	1465	6.00
6	9.40	34.1	760	Crosswind	5589	1.47	5189	631	20.70
7	10.90	22.0	586	Downwind	7211	357.40	6017	1643	5.54
8	11.88	27.2	#N/A	Upwind[3]	#N/A	#N/A	6558	#N/A	#N/A
9	12.98	19.5	442	Downwind	8738	0.08	7165	1807	4.01
10	13.97	22.1	487	Upwind	8690	0.05	7711	1696	0.07
11	14.98	0.9	296	Downwind[4]	9293	359.21	8269	1494	3.07
12	23.89	12.7	792	Cross/Upwind	14943	0.34	13187	934	5.90
13	25.18	1.9	466	Downwind	16318	357.68	13899	3386	3.24
14	26.63	1.1	258	Cross/Upwind[4]	16875	346.31	14700	1739	8.45
15	30.86	5.9	560	Cross/Upwind	20102	2.59	17035	2045	3.87
16	32.90	3.1	411	Partial Cross	21372	1.99	18161	1027	1.92
17	34.93	0.7	147	Cross/Upwind[4]	22612	343.99	19281	1192	6.35
18	36.32	0.2	458	Cross/Down[4]	20838	342.94	20049	589	5.93
19	38.68	9.4	495	Cross/Down	24923	3.29	21351	2460	9.12
20	40.60	0.6	536	Crosswind	24782	2.68	22411	1787	7.25
21	42.75	4.0	744	Crosswind	26118	358.73	23598	8	4.30
22	44.61	9.8	826	Crosswind	27400	358.60	24625	111	4.52
23	47.62	2.2	451	Cross/Upwind	30474	0.60	26286	2344	2.97
24	50.35	6.5	522	Crosswind	31942	1.28	27793	1626	5.30
25	52.10	8.3	541	Crosswind	32697	0.62	28759	1157	4.00
26	53.98	3.4	548	Crosswind	32304	358.76	29797	555	5.55
27	56.45	2.3	582	Crosswind	34317	357.32	31160	1290	6.45
28	58.35	2.7	553	Cross/Upwind	34768	359.14	32209	1438	2.61
29	59.42	4.2	517	Crosswind	36012	358.46	32800	1500	5.90
30	61.31	5.5	517	Crosswind	37412	358.72	33843	802	4.23
31	63.16	1.9	684	Crosswind	38178	356.53	34864	905	2.25
32	65.82	1.5	494	Peak on Plateau	41377	1.69	36333	1296	0.21
33	67.31	2.5	473	Upwind	41099	358.24	37155	761	0.56
34	71.74	3.3	442	Partial/Curve	45499	359.38	39600	2042	0.23
35	75.55	2.5	534	Partial/Curve	46955	358.16	41704	1227	1.97
36	81.05	1.2	559	Upwind	49773	355.72	44740	1403	1.05
37	83.93	0.9	583	Downwind	53126	354.97	46329	2456	1.18
38	86.50	3.0	678	Upwind	53867	353.27	47748	4798	1.80
39	89.02	1.8	640	Partial/Curve	55540	353.17	49139	3698	0.27
40	92.18	2.5	589	Cross/Upwind	58191	356.45	50883	1942	3.64
41	96.75	0.7	553	Cross/Upwind	61464	356.90	53406	1745	2.59

[1]The terms "crosswind" and "down/upwind" are used as relative labels and are not exact.

[2]The plume to pad distance was calculated using the imagery derived wind speed (9.2 meters/second).

[3]There was a gap in the aircraft data from t = 11.4 - 12.12 minutes.

[4]Detection of secondary cloud off main plume line.

Table 2. Aircraft-Derived Extent of the Titan IV #K15 Exhaust Cloud

No.	ts	te	Ds	De	θs	θe	Cloud Encounter w.r.t. Aircraft	
	start	end	start	end	start	end	Lp	θp
	(min)	(min)	(m)	(m)	(°)	(°)	(m)	(°)
1	3.846	4.067	1587	2580	357.77	355.42	996	351.69
2	4.933	5.246	2966	2579	349.38	9.55	1044	110.88
3	6.017	6.283	3701	3320	5.97	352.61	900	244.40
4	6.867	7.133	4250	4102	351.46	4.74	977	96.76
5	7.925	8.258	4182	5648	2.70	356.70	1551	340.33
6	9.163	9.754	5984	5353	354.27	14.97	2129	111.58
7	10.579	10.954	5792	7434	2.50	356.96	1761	338.45
8	11.612	12.246	8929	6299	0.06	359.35	2631	181.74
9	12.746	13.150	7715	9522	357.73	1.74	1904	18.21
10	13.675	14.192	9702	8006	359.93	0.00	1696	179.59
11	14.958	15.283	9221	10714	359.40	356.33	1585	338.19
12	23.642	24.133	15429	14496	357.70	3.60	1800	121.85
13	24.962	25.725	15277	18663	358.79	355.55	3518	341.35
14	26.438	27.296	17296	15558	348.25	339.80	2977	218.41
15	30.683	31.450	20548	18503	3.30	359.43	2432	214.19
16	32.688	32.979	20702	21730	0.33	2.25	#N/A	#N/A
17	34.733	35.513	22947	21755	345.42	339.07	2746	226.56
18	36.050	36.742	20526	21116	339.63	345.56	2233	57.31
19	38.100	39.267	23493	25954	358.77	7.89	4198	58.07
20	40.571	41.500	24728	26515	2.96	355.71	3698	298.17
21	42.583	43.100	26125	26133	357.34	1.64	1960	89.27
22	44.296	44.867	27742	27632	0.89	356.37	2186	265.72
23	47.262	48.192	31257	28913	2.00	359.03	2814	214.15
24	50.133	51.000	31451	33077	359.92	5.22	3397	64.00
25	51.896	52.550	32419	33576	2.03	358.03	2576	296.68
26	53.667	54.554	32499	31945	356.84	2.39	3169	99.68
27	55.663	56.692	33452	34742	2.44	355.99	4047	287.77
28	57.950	58.633	35599	34161	357.68	0.29	2142	131.12
29	58.975	59.996	35270	36770	1.06	355.16	3998	290.12
30	61.008	61.825	37667	36865	357.15	1.38	2865	105.51
31	62.913	63.342	37657	38562	357.83	355.58	1749	297.85
32	65.733	66.017	40993	42289	1.75	1.54	1305	354.94
33	67.183	67.467	41416	40655	358.46	357.90	860	206.00
34	71.142	72.038	46924	44883	358.63	358.40	#N/A	#N/A
35	74.896	75.862	48063	46836	358.73	356.76	#N/A	#N/A
36	80.600	81.146	50911	49508	356.57	355.52	1678	209.30
37	83.371	84.025	51049	53506	353.97	355.15	2682	18.23
38	85.629	87.254	56469	51671	354.36	352.56	5090	192.95
39	88.433	89.304	53034	56732	353.23	353.50	#N/A	#N/A
40	91.696	92.933	59130	57188	357.72	354.08	4173	238.18
41	96.350	97.400	62327	60581	357.67	355.08	3280	234.24

[1]The terms "crosswind" and "down/upwind" are used as relative labels and are not exact.

[2]The plume to pad distance was calculated using the imagery derived wind speed (9.2 meters/secon

[3]There was a gap in the aircraft data from t = 11.4 - 12.12 minutes.

[4]Detection of secondary cloud off main plume line.

Table 3. Aircraft-Derived Cloud Characteristics and Sampling Information

No.	Time of Pass at max. (min)	Peak HCl at max. (ppm)	Sampling Altitude at max. (meters)	Type of Pass[1]	Cloud Encounter w.r.t. Aircraft Lp (m)	Cloud Encounter w.r.t. Aircraft θp (°)	Cloud Speed based upon Max. SLC-4E (m/s)	Cloud Speed based upon Max. N/S (m/s)	Cloud Speed based upon Max. E/W (m/s)	Portion Sampled
1	4.03	37.2	910	Downwind	996	351.69	9.78	-9.75	0.72	E
2	5.15	42.2	949	Crosswind	1044	110.88	8.57	-8.56	-0.39	S
3	6.15	31.8	922	Crosswind	900	244.40	9.48	-9.48	0.09	S
4	7.00	31.8	898	Crosswind	977	96.76	9.81	-9.80	0.47	E
5	8.02	35.3	930	Downwind	1551	340.33	9.58	-9.58	-0.10	S
6	9.40	34.1	760	Crosswind	2129	111.58	9.91	-9.91	-0.25	S
7	10.90	22.0	586	Downwind	1761	338.45	11.03	-11.02	0.50	E
8	11.88	27.2	#N/A	Upwind[3]	2631	181.74	#N/A	#N/A	#N/A	S
9	12.98	19.5	442	Downwind	1904	18.21	11.22	-11.22	-0.02	S
10	13.97	22.1	487	Upwind	1696	179.59	10.37	-10.37	-0.01	S
11	14.98	0.9	296	Downwind[4]	1585	338.19	10.34	-10.34	0.14	S
12	23.89	12.7	792	Cross/Upwind	1800	121.85	10.42	-10.42	-0.06	S
13	25.18	1.9	466	Downwind	3518	341.35	10.80	-10.79	0.44	S
14	26.63	1.1	258	Cross/Upwind[4]	2977	218.41	10.56	-10.26	2.50	VE
15	30.86	5.9	560	Cross/Upwind	2432	214.19	10.86	-10.85	-0.49	W
16	32.90	3.1	411	Partial Cross	#N/A	#N/A	10.83	-10.82	-0.38	S
17	34.93	0.7	147	Cross/Upwind[4]	2746	226.56	10.79	-10.37	2.98	VE
18	36.32	0.2	458	Cross/Down[4]	2233	57.31	9.56	-9.14	2.80	VE
19	38.68	9.4	495	Cross/Down	4198	58.07	10.74	-10.72	-0.62	W
20	40.60	0.6	536	Crosswind	3698	298.17	10.17	-10.16	-0.48	W
21	42.75	4.0	744	Crosswind	1960	89.27	10.18	-10.18	0.23	S
22	44.61	9.8	826	Crosswind	2186	265.72	10.24	-10.24	0.25	S
23	47.62	2.2	451	Cross/Upwind	2814	214.15	10.67	-10.67	-0.11	S
24	50.35	6.5	522	Crosswind	3397	64.00	10.57	-10.57	-0.24	S
25	52.10	8.3	541	Crosswind	2576	296.68	10.46	-10.46	-0.11	S
26	53.98	3.4	548	Crosswind	3169	99.68	9.97	-9.97	0.22	S
27	56.45	2.3	582	Crosswind	4047	287.77	10.13	-10.12	0.47	E
28	58.35	2.7	553	Cross/Upwind	2142	131.12	9.93	-9.93	0.15	S
29	59.42	4.2	517	Crosswind	3998	290.12	10.10	-10.10	0.27	S
30	61.31	5.5	517	Crosswind	2865	105.51	10.17	-10.17	0.23	S
31	63.16	1.9	684	Crosswind	1749	297.85	10.07	-10.05	0.61	E
32	65.82	1.5	494	Peak on Plateau	1305	354.94	10.48	-10.48	-0.31	S
33	67.31	2.5	473	Upwind	860	206.00	10.18	-10.18	0.31	S
34	71.74	3.3	442	Partial/Curve	#N/A	#N/A	10.57	-10.57	0.11	S
35	75.55	2.5	534	Partial/Curve	#N/A	#N/A	10.36	-10.35	0.33	S
36	81.05	1.2	559	Upwind	1678	209.30	10.24	-10.21	0.76	E
37	83.93	0.9	583	Downwind	2682	18.23	10.55	-10.51	0.92	E
38	86.50	3.0	678	Upwind	5090	192.95	10.38	-10.31	1.22	VE
39	89.02	1.8	640	Partial/Curve	#N/A	#N/A	10.40	-10.33	1.24	VE
40	92.18	2.5	589	Cross/Upwind	4173	238.18	10.52	-10.50	0.65	E
41	96.75	0.7	553	Cross/Upwind	3280	234.24	10.59	-10.57	0.57	E

[1]The terms "crosswind" and "down/upwind" are used as relative labels and are not exact.

[2]The plume to pad distance was calculated using the imagery derived wind speed (9.2 meters/second).

[3]There was a gap in the aircraft data from t = 11.4 - 12.12 minutes.

[4]Detection of secondary cloud off main plume line.

3.3 Summary Plots of Aircraft Geomet HCl Data (100 minute Interval)

The previous section and the appendices graphically documented and parametrized the available data in great detail. This portion of the results uses graphical methods to review trends and correlations between the measured HCl concentrations and the various sampling parameters. Filters (i.e., ranges of parameters) are used to reduce the data prior to comparison against model predictions. The filtered data are compared not only to REEDM predictions but also to previous imagery-derived results.

We will start with a series of plots that graphically document the entire dataset (i.e., Figures 19 through 23). Figures 19 through 22 include maximum HCl concentration plotted against time. The HCl concentration data are labeled according to the angular position of the maximum hit relative to a due south trajectory. A filled square represents a hit that was due south (i.e., labeled "S" in the plot) and had a east/west component of velocity between ±0.45 m/s. A filled diamond represents a hit that was slightly to the west of due south (i.e., labeled "W" in the plot) and had a east/west component of velocity more negative than –0.45 m/s. A circle represents a hit that was very east of due south (i.e., labeled "VE") and had an east/west component of velocity more positive than 1.0 m/s. Finally, a triangle represents a hit that was slightly to the east of due south (i.e., labeled "E" in the plot) and had an east/west component of velocity between +0.45 and +1.00 m/s. In addition to the HCl concentration data (i.e., "Peak HCl" plotted against "Time of Pass" and labeled by the "Portion Sampled"), Figure 19 includes the altitude of the maximum hit; Figure 20 includes the apparent cloud speed needed to reach the position of the maximum hit by the time of the maximum hit; Figure 21 includes the distance of the hit relative to the distance of the average cloud (i.e., the difference between the apparent speed for any hit versus the average speed of all hits converted to distance using the sampling time); Figure 22 includes the length of the encounter. In Figure 21, positive values for the differences indicate that the hit was leading (i.e., further from the source) the average cloud, while negative values for the difference indicate that the hit was tailing (i.e., closer to the source) the average cloud. As mentioned previously, one must assume that the pilot targeted the middle of the cloud most of the time and that the cloud traveled at a relatively constant rate. These are reasonable assumptions. These various parameters were included to illustrate the complexity of the dataset and to allow the filtering of the data for comparison with models.

Figure 23 is a Cartesian plot and documents the length and direction of each encounter by plotting the start and end (connected by a line) for each of the 41 passes. It is apparent that the extent of the encounters varied dramatically and that the hits shifted to the southeast at greater distances. *Review of Figure 17 in the previous report[4] on the #K15 mission, reveals that the aircraft did not sample the western quadrant at distances greater than 44,000 m and did not sample due south of the pad at distances greater than 49,000 m. Therefore, the apparent shift in cloud trajectory merely reflects the fact that the aircraft only sampled the eastern quadrant at later times.*

At best, the aircraft can measure the widest extent of the cloud. However, review of Figures 19 through 23 reveals that most of the time the aircraft sampled only a portion of the cloud. In Figure 24, the Geomet-derived crosswind width (i.e., the length of the encounter for crosswind passes) is plotted against time. By fitting only the extremes of these crosswind data, we obtain an apparent expansion rate. Likewise, in Figure 25, the Geomet-derived start of each encounter is plotted on a Cartesian grid. The data are labeled differently for the eastern and western edges. By plotting only

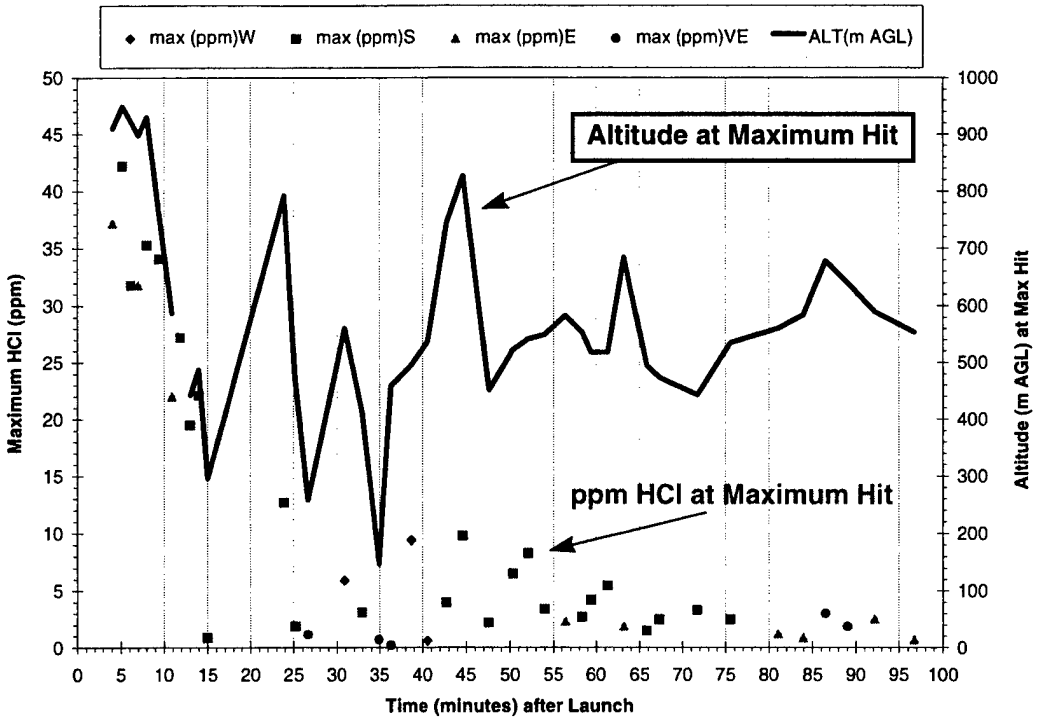

Figure 19. Altitude and HCl concentration plotted against time (0 to 100 min).

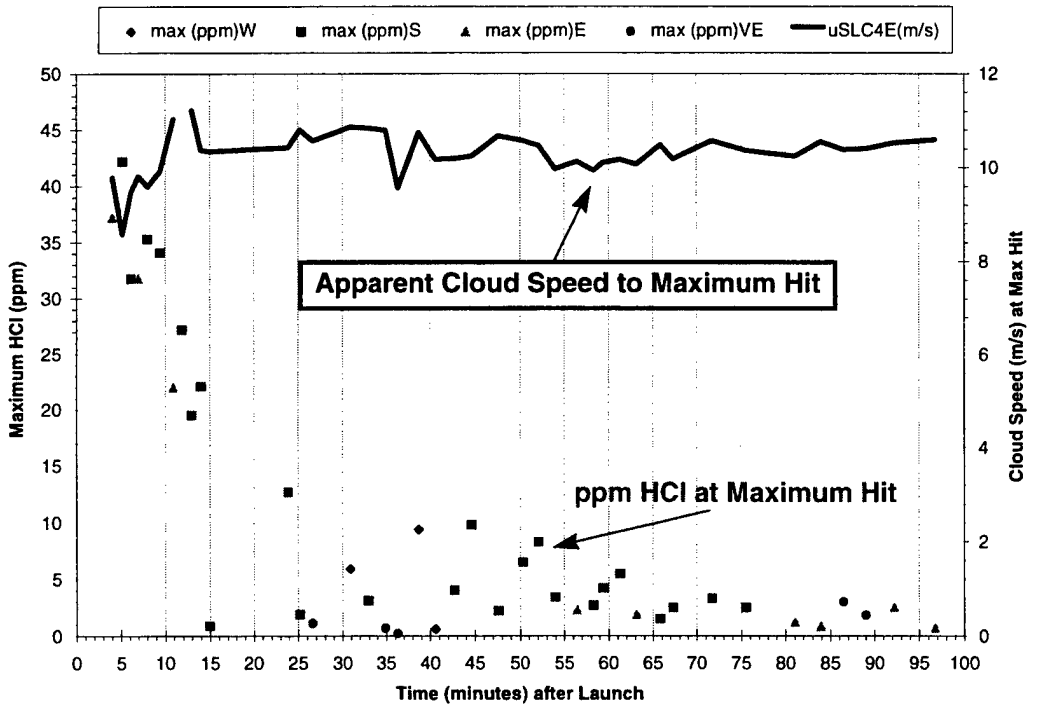

Figure 20. Apparent cloud speed and HCl concentration plotted against time (0 to 100 min).

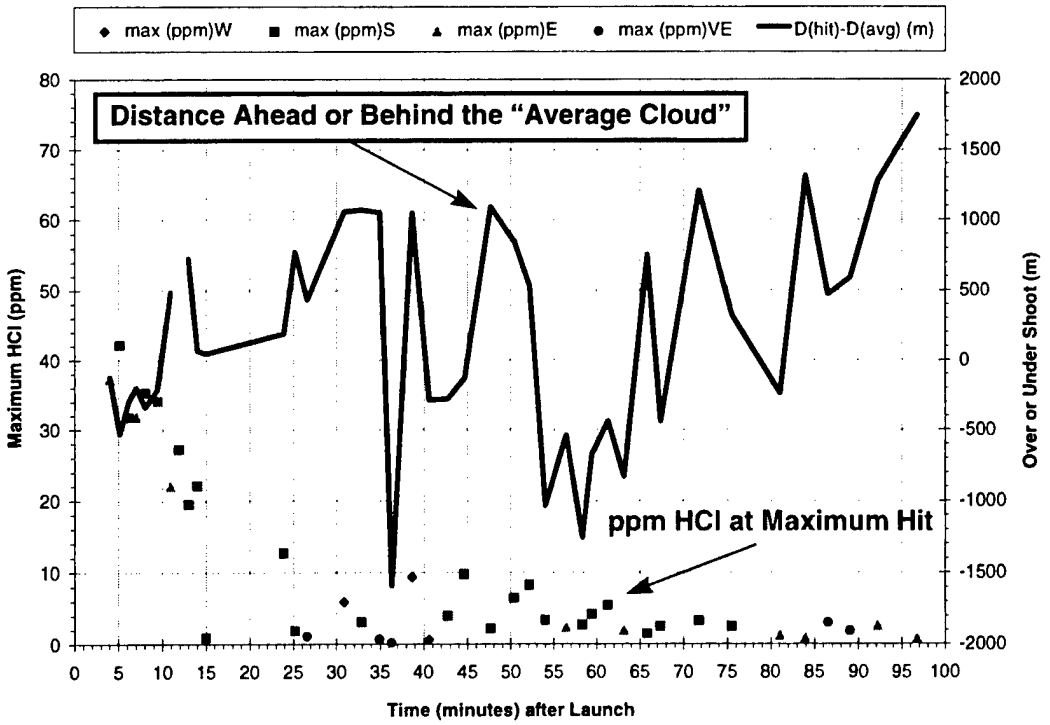

Figure 21. Relative Distance of Maximum Hit plotted with HCl concentration (0 to 100 min).

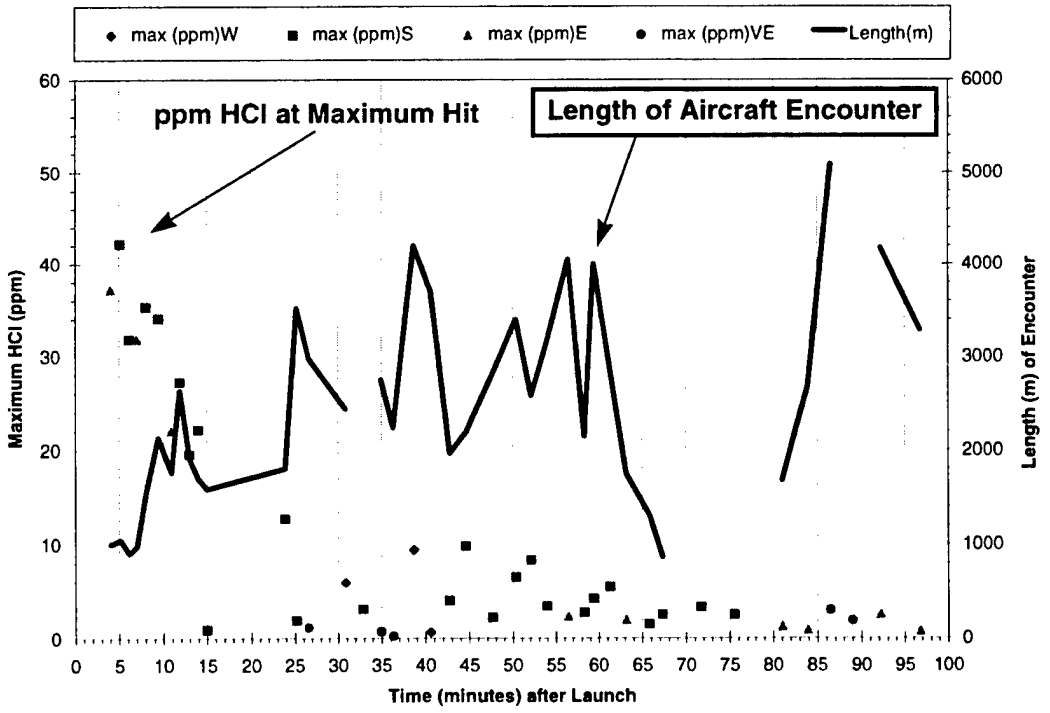

Figure 22. Length of encounter plotted with HCl concentration (0 to 100 min).

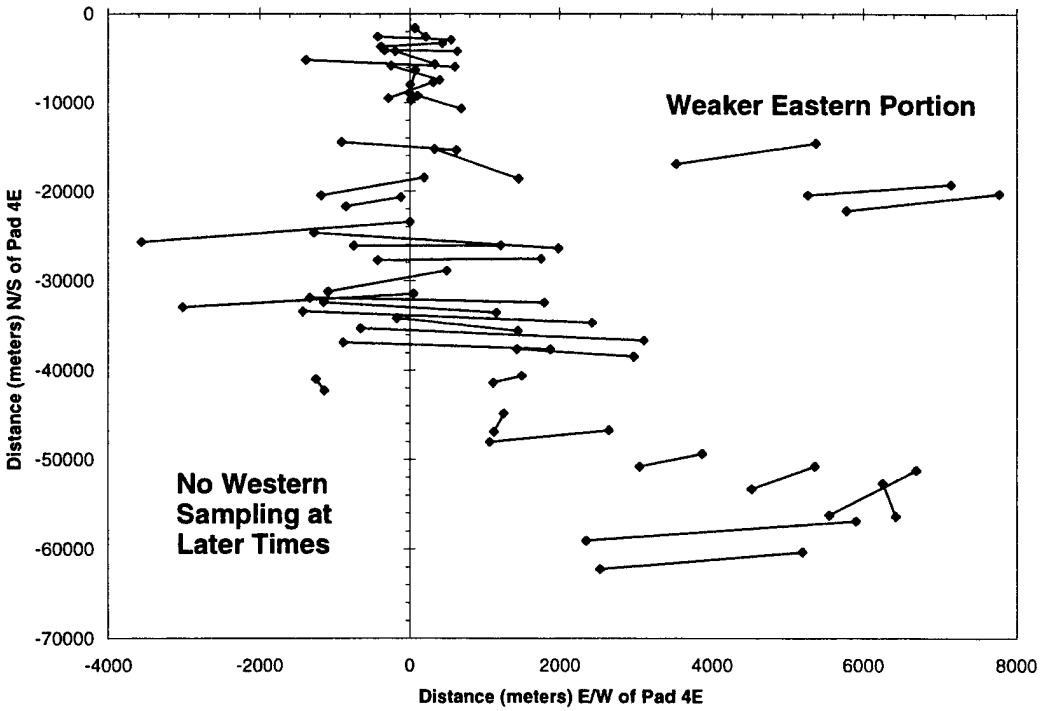

Figure 23. Cartesian plot of Geomet-derived cloud extent (0 to 100 min).

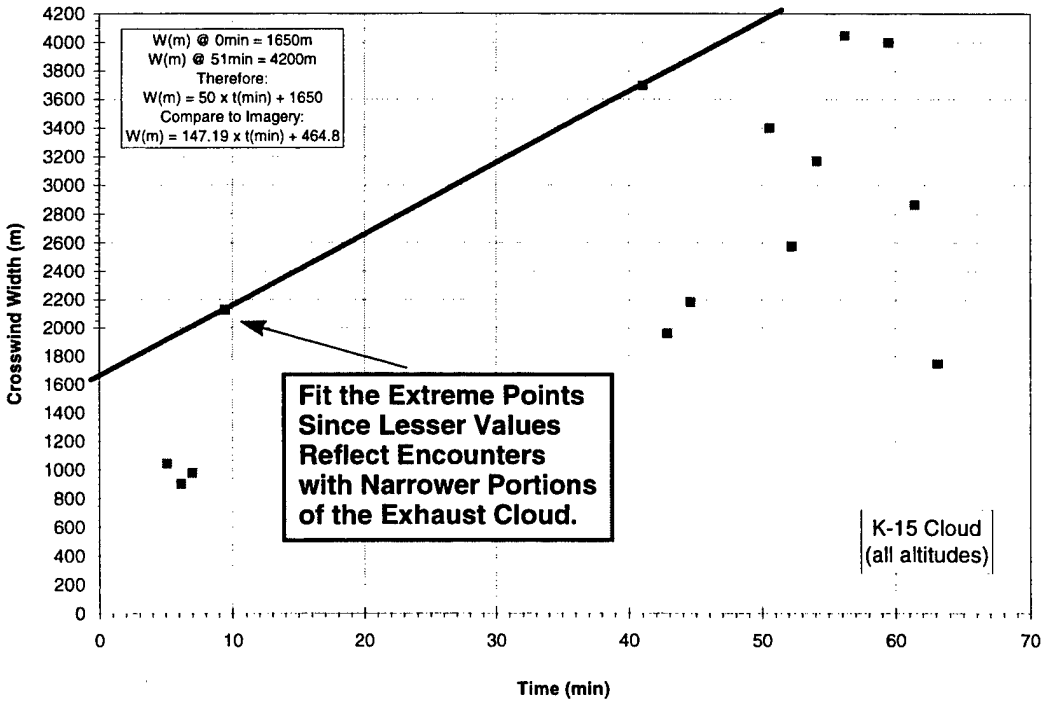

Figure 24. Geomet-derived crosswind width plotted against time (0 to 100 min).

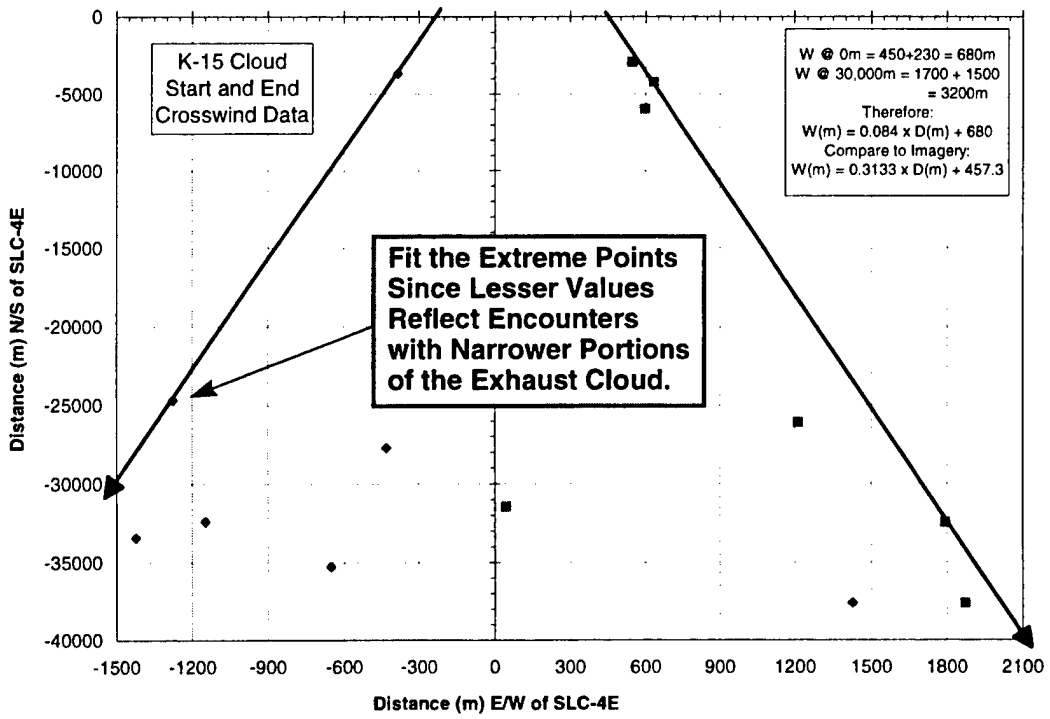

Figure 25. Cartesian plot of Geomet-derived cloud extent (only start points).

the start of the hit, we avoid any confusion associated with the slow recovery (i.e., tail) of the Geomet. Again, by using only the extremes of these crosswind data, we obtain an apparent expansion rate. In both Figures 24 and 25, a text box reports the formula for the Geomet-derived and imagery-derived expansion with time and distance, respectively. It is interesting to note that the Geomet-derived slopes are about a third of the imagery-derived slopes in both of these figures. Since the method used in Figure 24 includes the Geomet-derived end (i.e., may include recovery slope errors) while the method used in Figure 25 avoided those potential errors, one can infer that the analyst did a reasonable job of selecting the end of the cloud. One can infer, from the small value of the expansion rate, that the aircraft sampled only a portion of the cloud at later times.

Figure 26 presents a time plot of all of the HCl data with the most significant sampling parameters while Figure 27 uses the same format but includes only the data that met the following restrictions to the sampling parameters: (1) only include hits at altitudes greater than 400 m AGL, (2) only include hits that have apparent cloud speeds within one standard deviation (i.e., ±0.48 m/s) of the average cloud speed (i.e., 10.29 m/s based upon the maxima of all 41 passes); and (3) only include the encounters that represent the maximum length relative to neighboring hits. The filtering of the data resulted in seven encounters with the cloud with the following type distribution: four crosswind, one upwind, one cross/upwind, and one cross/downwind. In spite of the assortment in type, the time decay of the HCl concentration is fit nicely by the third-order polynomial drawn in Figure 27.

Figure 28 is a time plot that allows direct comparison of REEDM 7.07 (lines in the upper plot), REEDM 7.08 (lines in the lower plot), and filtered aircraft data (symbols in both plots). The solid lines represent REEDM predictions for the Peak HCl concentration at the predicted stabilization

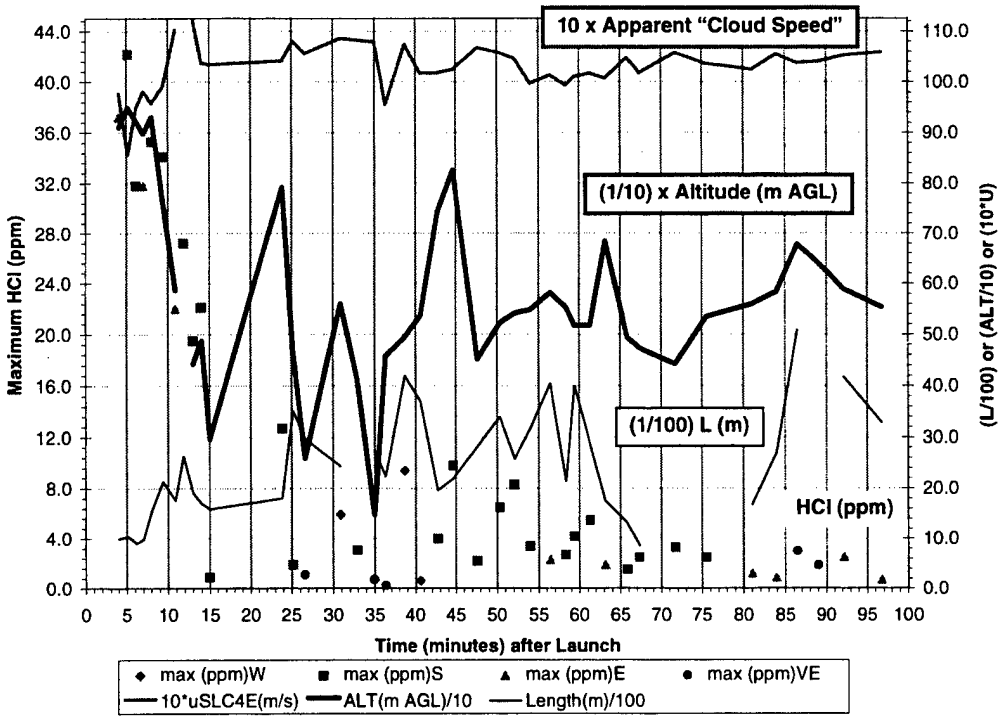

Figure 26. Correlation plot for [HCl], altitude, speed, and length of encounter (0 to 100 min).

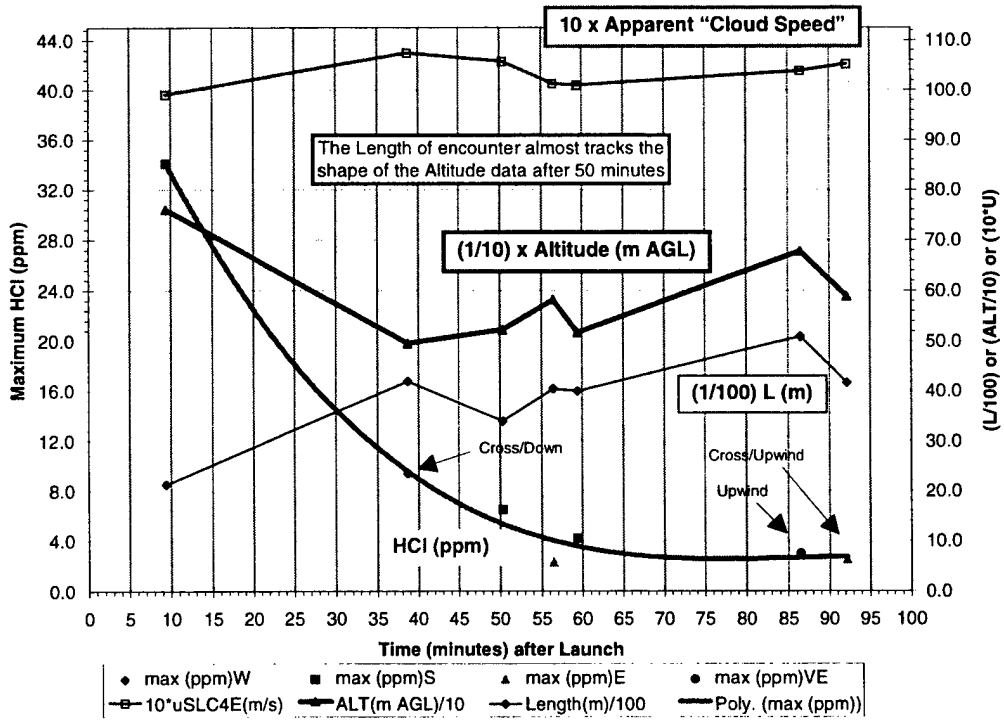

Figure 27. Filtered Correlation plot for [HCl], altitude, speed, and length (0 to 100 min).

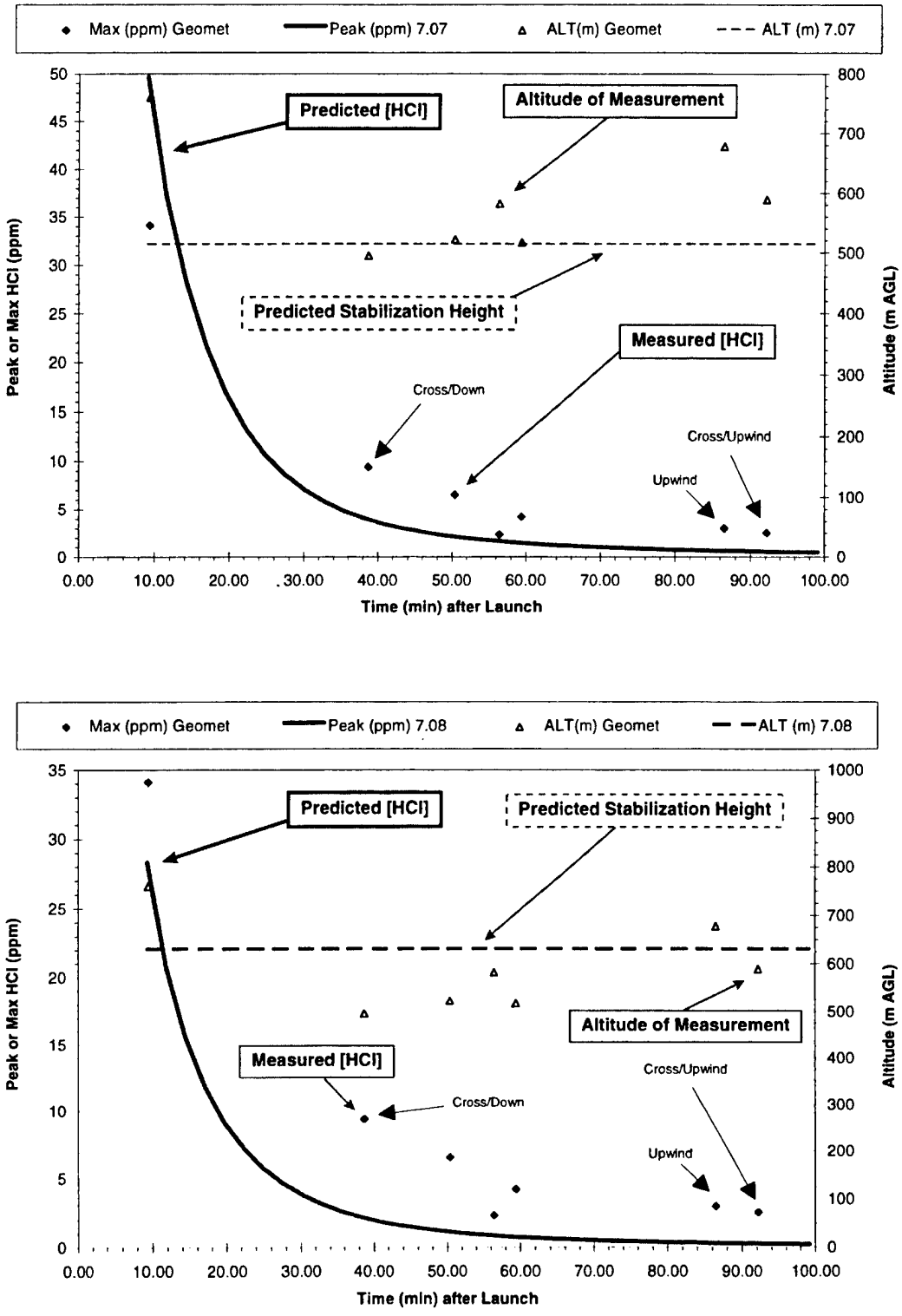

Figure 28. Aircraft data compared to REEDM 7.07 (upper) and 7.08 (lower) predictions.

height. The dashed lines represent REEDM predictions for the stabilization height. The filtered aircraft data use diamonds as labels for the maximum HCl concentration for each encounter and triangles as labels for the aircraft's sampling altitude at the maximum HCl hit. Figure 28 reveals that the Geomet reported greater HCl concentrations than predicted by either version of REEDM (using default inputs tabulated later in this report). This is surprising since the aircraft sampled at altitudes scattered about the predicted stabilization height and, therefore, should have reported lower concentrations.

Figure 29 documents the absolute (upper plot) and percent (lower plot) difference between the measured (i.e., the polynomial fit to the filtered aircraft data in Figure 27) and the predicted HCl concentrations at the stabilization height (i.e., the REEDM predictions plotted in Figure 28). In Figure 29, a zero value represents agreement with the polynomial fit to the measured trend. The upper plot reveals 2 to 15 ppm differences between REEDM and the aircraft data. Both versions of REEDM underpredict the HCl concentration at later times. It is apparent from the lower plot that REEDM's predicted concentrations are only 10 to 20% (i.e., –90 to –80% difference) of the measured values at times longer than 40 min. This is in spite of the Geomet's 18-s sampling period, which would tend to minimize the differences (i.e., the Geomet should report a lower-than-actual HCl concentration when there are rapid changes in concentration).

Table 4 summarizes not only the input (columns 2 through 4) and output (columns 5 through 9) for various REEDM runs but also the measured cloud characteristics (i.e., imagery and aircraft Geomet). The imagery documented the initial cloud radius (ri), the initial cloud height (Hi), and the stabilization heights for the #K15 mission. The imagery-derived entrainment coefficient (γ) is 0.35 based upon two Titan IVA launches (#K19 and #K23), one Titan IVB launch (#K24), and one Titan 34 abort (D-9). The aircraft's Geomet-derived HCl concentrations were calculated using the polynomial fit to the filtered aircraft data (Figure 27) and an average speed of 10.29 m/s (i.e., average speed for all aircraft-encounter maxima). Therefore, 30 km corresponds to 48.59 min using the average speed and 5.78 ppm using the time-dependent polynomial fit. A distance of 60 km corresponds to 97.18 min using the average speed and 2.65 ppm using the time-dependent polynomial fit.

It is readily apparent from Table 4 that all REEDM predictions are dramatically low for the HCl concentration at 30 and 60 km downwind. As discussed previously, the REEDM predictions for the HCl concentrations are at the stabilization height (i.e., maximum possible at the specified distances). This is probably not the case for the aircraft transects. Likewise, the Geomet reports a lower-than-actual concentration based upon its response function and calibration data.

In addition to underestimating the HCl concentration, Table 4 documents dramatic differences for the vertical extent of the cloud at stabilization time (i.e., heights of the bottom and top) and for the cloud's stabilization height (i.e., middle). The default values for the three input parameters were 71.99 for ri, 0 for Hi, and 0.64 for the entrainment coefficient in our copies of REEDM 7.07 and 7.08. These default values were used in the first run of each version of REEDM that was reported in Table 4. These default values were used for the runs plotted in the figures in this and the previous reports. *The recently proposed defaults are 71.99 for ri, 71.99 for Hi, and 0.64 for the entrainment coefficient. It is apparent from review of Table 4 that these new default values affect the stabilization height and extent at stabilization time but do not significantly affect the downrange HCl*

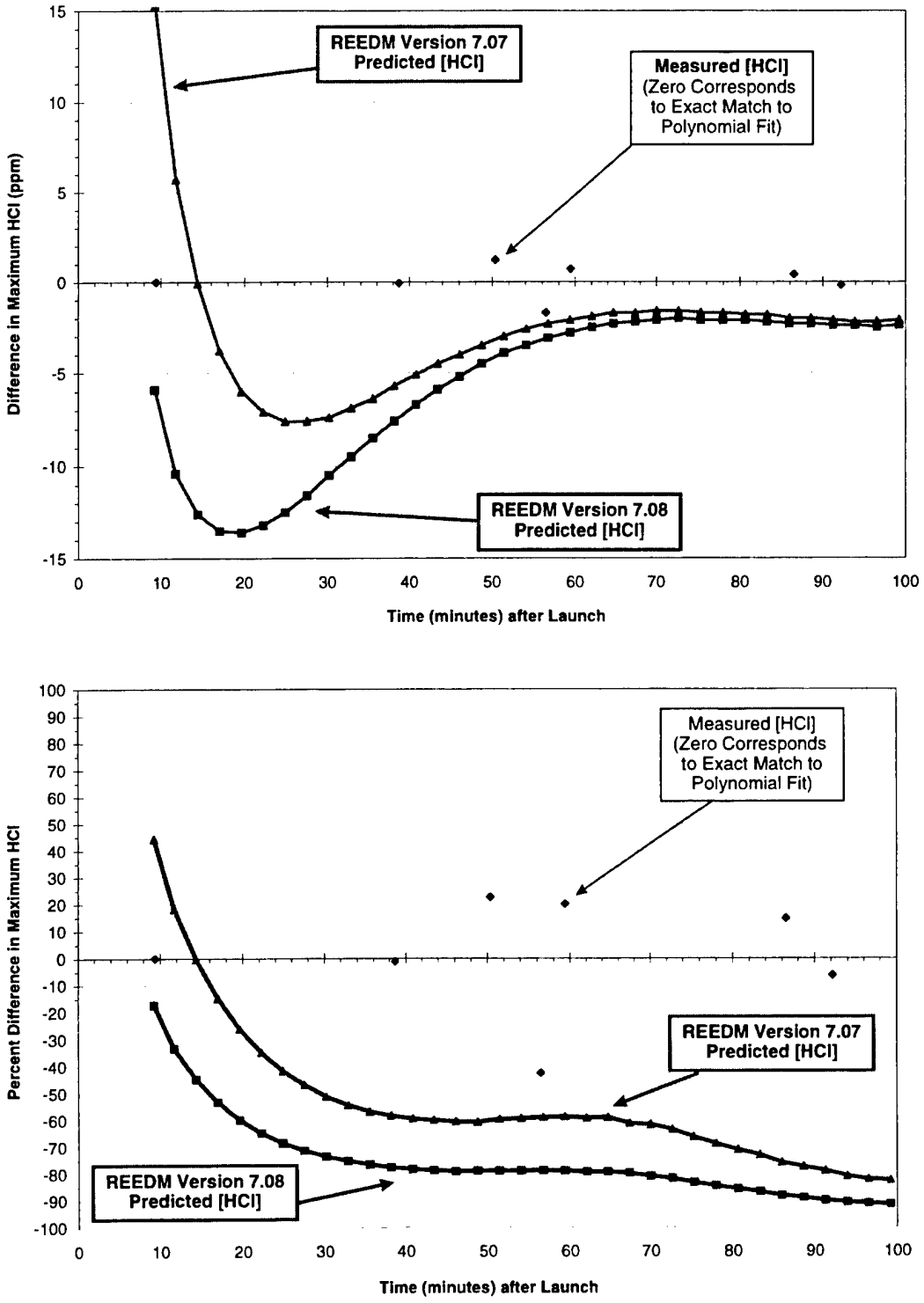

Figure 29. Error estimates as absolute difference (upper) and percent difference (lower).

Table 4. Measured and Predicted Cloud Characteristics

Source	ri (m)	Hi (m)	γ	H_{bottom} (m)	H_{middle} (m)	H_{top} (m)	ppm @ 30km	ppm @ 60km
REEDM 7.07	71.99	**0**	0.64	169	515	994	**0.78**	0.08
REEDM 7.07	71.99	71.99	0.64	200	**651**	**1168**	0.72	**0.15**
REEDM 7.08	71.99	**0**	0.64	199	**631**	**1168**	0.39	0.08
REEDM 7.08	71.99	71.99	0.64	312	796	1341	0.39	0.07
REEDM 7.08	71.99	71.99	**0.35**	824	1444	1999	0.55	0.08
REEDM 7.08	165	50	**0.35**	**400**	**624**	994	0.40	0.08
REEDM 7.08	**230**	**0**	**0.35**	169	303	425	0.50	0.08
Imagery	230	0	0.35	383 +/- 31	658 +/- 48	1172 +/- 98	na	na
Geomet	na	na	na	na	na	na	5.78	2.65

concentrations. It is also apparent from review of Table 4 that the imagery and aircraft data are complimentary and essential for validating dispersion models.

Figure 30 documents the extent of the cloud as a function of time and, hence, the expansion rate for the cloud. Figure 30 includes the filtered aircraft-derived cloud encounter lengths (as symbols) and the imagery-derived crosswind expansion rate (i.e., extrapolated from 6.5 min as a dot-dash line). A solid line connects the two extreme aircraft points and defines the maximum aircraft-derived expansion rate. For comparison, these plots also include the predicted alongwind expansion rate from REEDM 7.07 (dashed line in the upper plot) and from REEDM 7.08 (dashed line in the lower plot). The REEDM expansion rates were approximated from tabular output for the exhaust cloud. The REEDM output tabulates the arrival and departure times for various ranges from the launch pad. We calculated the length of the cloud as the difference in range between table entries that had equivalent arrival and departure times. A plot of this difference in range against time provided an apparent alongwind expansion rate. That straight line is included in Figure 30.

It is apparent from Figure 30 that the imagery, the aircraft data, and both versions of REEDM nearly agree only at 10 min. At later times, the extrapolated imagery-derived expansion rate is dramatically greater than any of the later aircraft encounters and either of the REEDM predictions. One must remember that the filtered aircraft data includes crosswind, along wind, and diagonal passes relative to the southerly cloud bearing. This mixed set of data could account for the scatter in the aircraft data. It is interesting to note that the maximum crosswind expansion rate derived from the unfiltered aircraft data (Figure 24) is lower than the maximum rate derived from the filtered data (i.e., solid line in Figure 30). At 40 min, the filtered crosswind cloud diameter would be 3650 m (i.e., 50 x 40 + 1650) whereas Figure 30 documents a cloud diameter closer to 4400 m (solid line at 40 min). The fact that the aircraft data fall below REEDM predictions is consistent with the fact that the aircraft sampled only a portion of the cloud at later times. This was demonstrated previously by Figure 23. It appears that REEDM version 7.08 provides a more realistic expansion rate based upon the extrapolated imagery-derived rate and agreement with the maximum aircraft-derived rate. However, the #K15 data cannot substantiate the actual expansion rate at times greater than 10 min (i.e., when there is no complimentary imagery data). At later times, we cannot verify that the aircraft sampled the fullest extent of the cloud, and, indeed, the data documents that it did not.

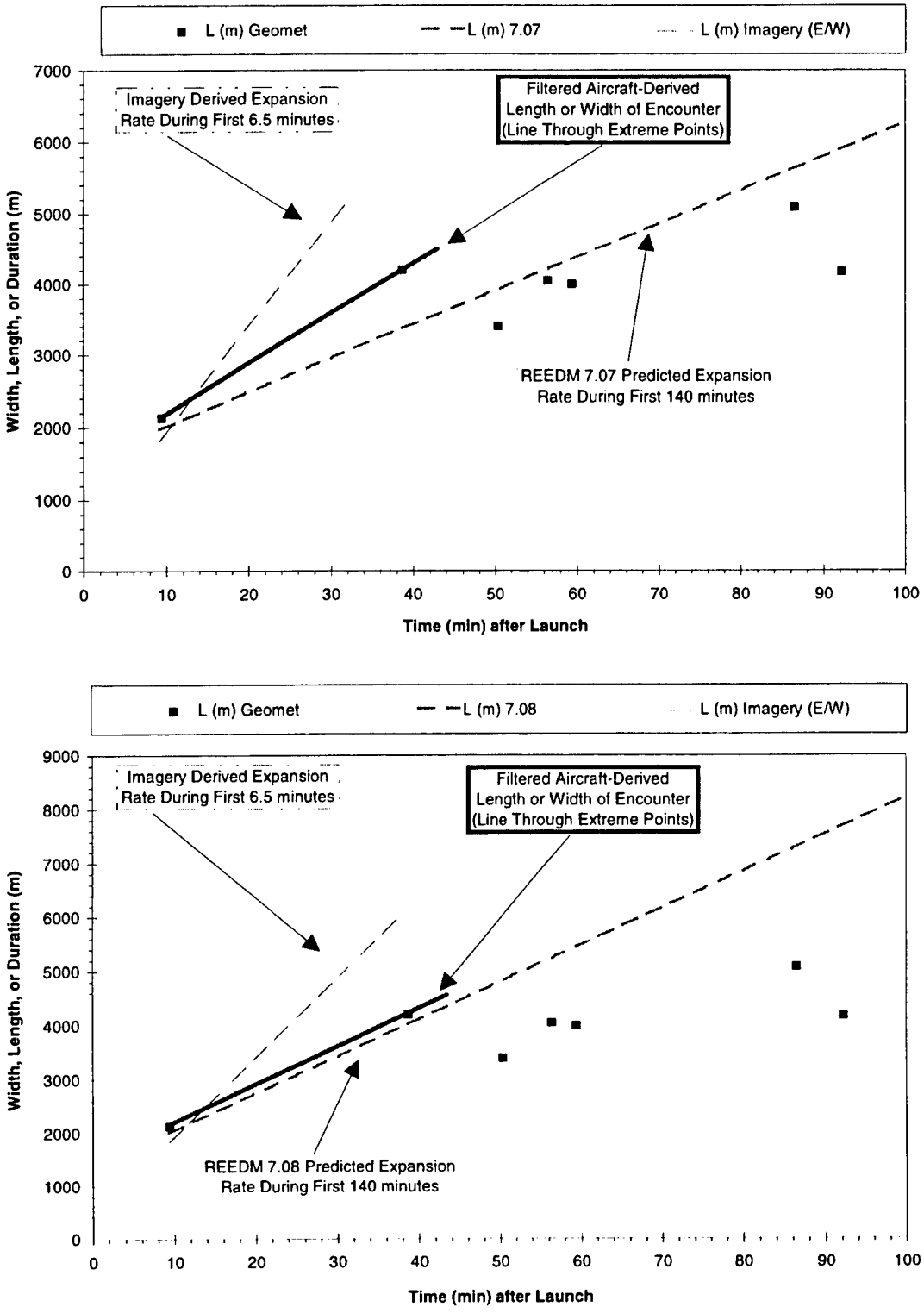

Figure 30. Expansion rates compared to REEDM 7.07 (upper) and 7.08 (lower) predictions.

4. Conclusions

The combination of IR and visible imagery with aircraft sampling provided a three-dimensional picture of the Titan IV #K15 exhaust cloud for the first 10 min after launch. Review of these complimentary data revealed excellent edge detection, both by the imagery and by the aircraft's Geomet HCl monitor. The imagery documented that the aircraft sampled the middle portion of the exhaust cloud during its first six encounters. The aircraft-derived exhaust cloud width is comparable to the imagery-derived exhaust cloud width only at these early times. At later times, the aircraft sampling provided HCl concentration profiles that documented peak HCl concentrations greater than predicted by REEDM versions 7.07 or 7.08. However, the aircraft did not map the full extent of the ground cloud at later times. In addition to documenting higher-than-predicted HCl concentration at times greater than 40 min, the aircraft mapped the edge of the cloud in the southwest quadrant for 95 min after launch. The aircraft data document that the ground cloud fragments into parcels that disperse more slowly than predicted.

It is important to remember that the aircraft's Geomet detector recovered to baseline quickly after each encounter, and, therefore, mapped regions not occupied by the exhaust cloud. It is important to compare model predictions not only to the measured HCl concentrations within the cloud but also to the zero concentrations outside of the cloud. To this end, the aircraft's data is available in electronic form. This will allow rigorous comparison to model predictions using the aircraft's sampling positions as point receptors (i.e., latitude, longitude, altitude, and time). Three-dimensional plotting can also be used to compare model predictions to aircraft measurements.

References

1. Environmental Systems Directorate, "Ground Cloud Dispersion Measurements During the Titan IV #K23 (14 May 1995) at Cape Canaveral Air Station: Volume 1—Test Overview and Data Summary," Aerospace Report No. TR-96(1410)-1, SMC-TR-96-01, The Aerospace Corporation, El Segundo, CA (27 February 1996).

2. Environmental Systems Directorate, "Ground Cloud Dispersion Measurements During the Titan IV #K19 (10 July 1995) at Cape Canaveral Air Station," Aerospace Report No. TR-96(1410)-3, SMC-TR-96-18, The Aerospace Corporation, El Segundo, CA (22 March 1996).

3. Environmental Systems Directorate, "Ground Cloud Dispersion Measurements During the Titan IV #K21 (6 November 1995) at Cape Canaveral Air Station," Aerospace Report No. TR-96(1410)-4, SMC-TR-96-21, The Aerospace Corporation, El Segundo, CA (21 June 1996).

4. Environmental Systems Directorate, "Ground Cloud Dispersion Measurements During The Titan IV Mission #K15 (5 December 1995) at Vandenberg Air Force Base, Volume 1—Test Overview and Data Summary," Aerospace Report No. TR-97(1410)-3, SMC-TR-97-05, The Aerospace Corporation, El Segundo, CA (10 February 1997).

5. Environmental Systems Directorate, "Ground Cloud Dispersion Measurements During the Titan IV #K16 (24 April 1996) at Cape Canaveral Air Station, Volume 1—Test Overview and Data Summary," Aerospace Report No. TR-97(1410)-4, SMC-TR-97-10, The Aerospace Corporation, El Segundo, CA (31 March 1997).

6. Environmental Systems Directorate, "Ground Cloud Dispersion Measurements During the Titan IV #K22 (12 May 1996) at Vandenberg Air Force Base, Volume 1—Test Overview and Data Summary," Aerospace Report No. TR-97(1410)-5, SMC-TR-97-18, The Aerospace Corporation, El Segundo, CA (30 June 1997).

7. Environmental Systems Directorate, "Ground Cloud Dispersion Measurements During the Titan IV Mission #K2 (3 July 1996) at Cape Canaveral Air Station, Volume 1—Test Overview and Data Summary," Aerospace Report No. TR-97(1410)-6, SMC-TR-97-19, The Aerospace Corporation, El Segundo, CA (15 July 1997).

8. R. N. Abernathy, R. F. Heidner III, B. P. Kasper, and J. T. Knudtson, "Visible and Infrared Imagery of the Launch of Titan IV K-23 from Cape Canaveral Air Force Station on 14 May 1995," Aerospace Report No. TOR-96(1410)-1, The Aerospace Corporation, El Segundo, CA (15 September 1996).

9. R. N. Abernathy, R. F. Heidner III, and K. L. Foster, "Aircraft HCl Sampling of the Titan IV K-23 Launch Effluent Cloud," Aerospace Report No.TR-96(1410)-2, SMC-TR-96-22, The Aerospace Corporation, El Segundo, CA (15 September 1996).

10. R. N. Abernathy, "Titan 34D-9 Abort Cloud Measurements—Quantitative Imagery from Two Camera Sites," Aerospace Report No. TR-98(1410)-1, The Aerospace Corporation, El Segundo, CA (20 February 1998).

Appendix A—Acronyms and Abbreviations

AGL	Above Ground Level (SLC-4E is ground level for the abort cloud)
Alt	Altitude in meters above specified reference (i.e., SLC-4E for 34D-9 cloud)
AZ	Azimuth clockwise from north
CCAS	Cape Canaveral Air Station
dAZ	Difference in AZ between two objects in an image
dEL	Difference in EL between two objects in an image
dW	Difference in absolute Width (i.e., corrected for FOV) for an object observed in different images
dX	Difference in X pixel values between two pixels (i.e., objects in an image)
dY	Difference in Y pixel values between two pixels (i.e., objects in an image)
D	ground Distance between two objects
EL	Elevation of object relative to level
FOV	Field Of View of image in degrees horizontal or degrees vertical
GMT	Greenwich Mean Time
Ground Cloud	normal launch cloud that includes exhaust reflected from pad and launch column consumed by rising exhaust duct cloud
LBS	pounds
mean	weighted average of all values
middle	half way between the top and the bottom and half way between the left and the right
MSL	Mean Sea Level
MST	Mobile Service Tower at launch pad
MVP	Model Validation Program
N_2O_4	dinitrogen tetroxide (i.e., hypergolic oxidizer)
PST	Pacific Standard Time
PSIA	Pounds per Square Inch Absolute
REEDM	Rocket Exhaust Effluent Dispersion Model used at VAFB and CCAS
SLC	Space Launch Complex
SR	Slant Range between imagery site and observed feature
SRM	Solid Rocket Motor
TVC	Thrust Vector Control

UT	Umbilical Tower at launch pad
VAFB	Vandenberg Air Force Base
x	Cartesian coordinate in east/west direction relative to SLC-4E at x,y = 0,0
X	"horizontal" pixel value (i.e., 0 at left of image and 640 at right of image)
y	Cartesian coordinate in north/south direction relative to SLC-4E at x,y = 0,0
Y	"vertical" pixel value (i.e., 0 at bottom of image and 480 at top of image)
z	altitude relative to MSL (opposed to "Alt" which is relative to SLC-4E)

Appendix B—10-Min Plots for Aircraft Data

The following figures document the aircraft's position and the Geomet's HCl measurements using two plots for each 10-min period. During the first 11 min after launch, the quantitative imagery of the entire exhaust cloud was combined with the aircraft transits through portions of the exhaust cloud to generate a 3-D picture of the ground cloud. As discussed in the results section of this report, the imagery-derived extent of the cloud provided an outline of the cloud and allowed the interpretation of the aircraft's Geomet-derived HCl concentrations as transits through the middle portion of the ground cloud. There is no quantitative imagery for times longer than 11 min, but the aircraft sampled the ground cloud for 100 min. Therefore, one needs to analyze the aircraft data to determine its utility for mapping of the ground cloud trajectory and extent without complimentary imagery.

As discussed in the results section of this report, Appendix B contains two plots for each 10 min of aircraft data (i.e., 0–10, 10–20, through 90–100 min). The two plots provided for each 10 min of flight are:

- A time plot documenting the aircraft altitude and the strength of the Geomet's HCl measurements (also, when available, the imagery-derived altitudes for the top and bottom of the ground cloud)

- A Cartesian plot documenting the location and the strength of the Geomet's HCl measurements.

The results section discusses not only these plots but also provides tabular and graphical analysis of these aircraft data. We provide these plots to allow direct comparison with REEDM output. These data are available as ASCII comma-separated variable files to facilitate more rigorous comparisons.

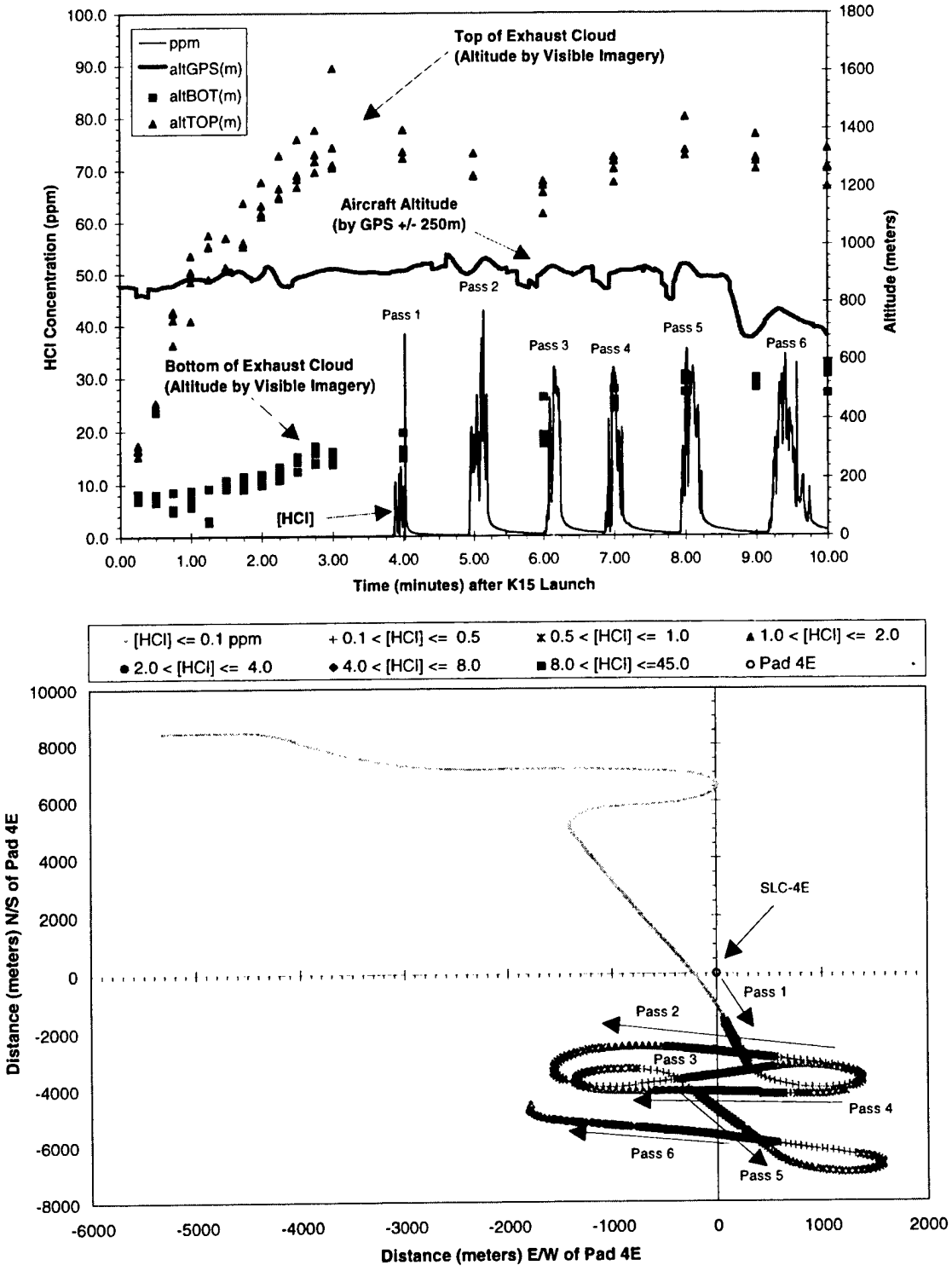

Figure B-1. Time and Cartesian Plots for Passes 1–6.

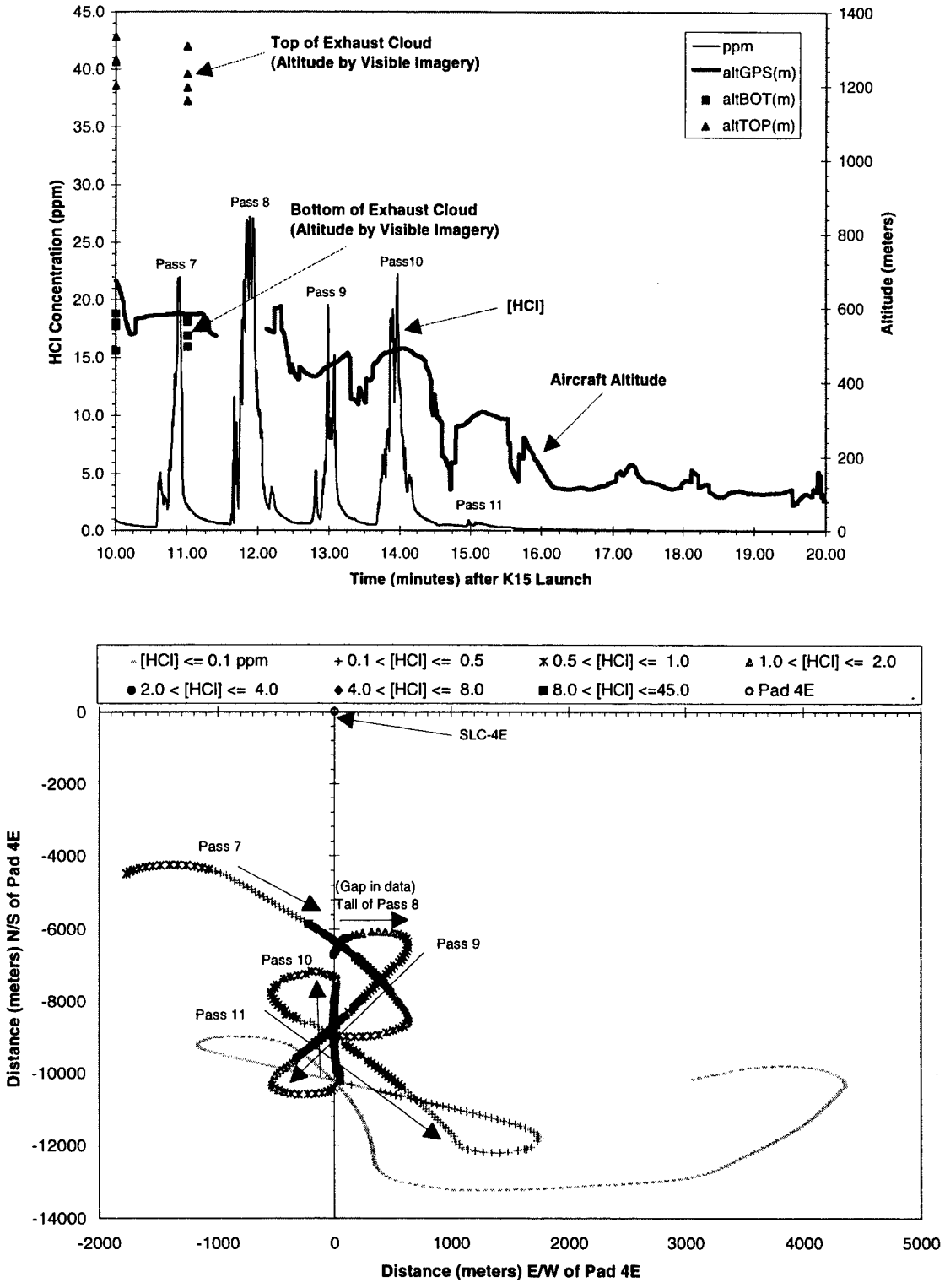

Figure B-2. Time and Cartesian Plots for Passes 7–11.

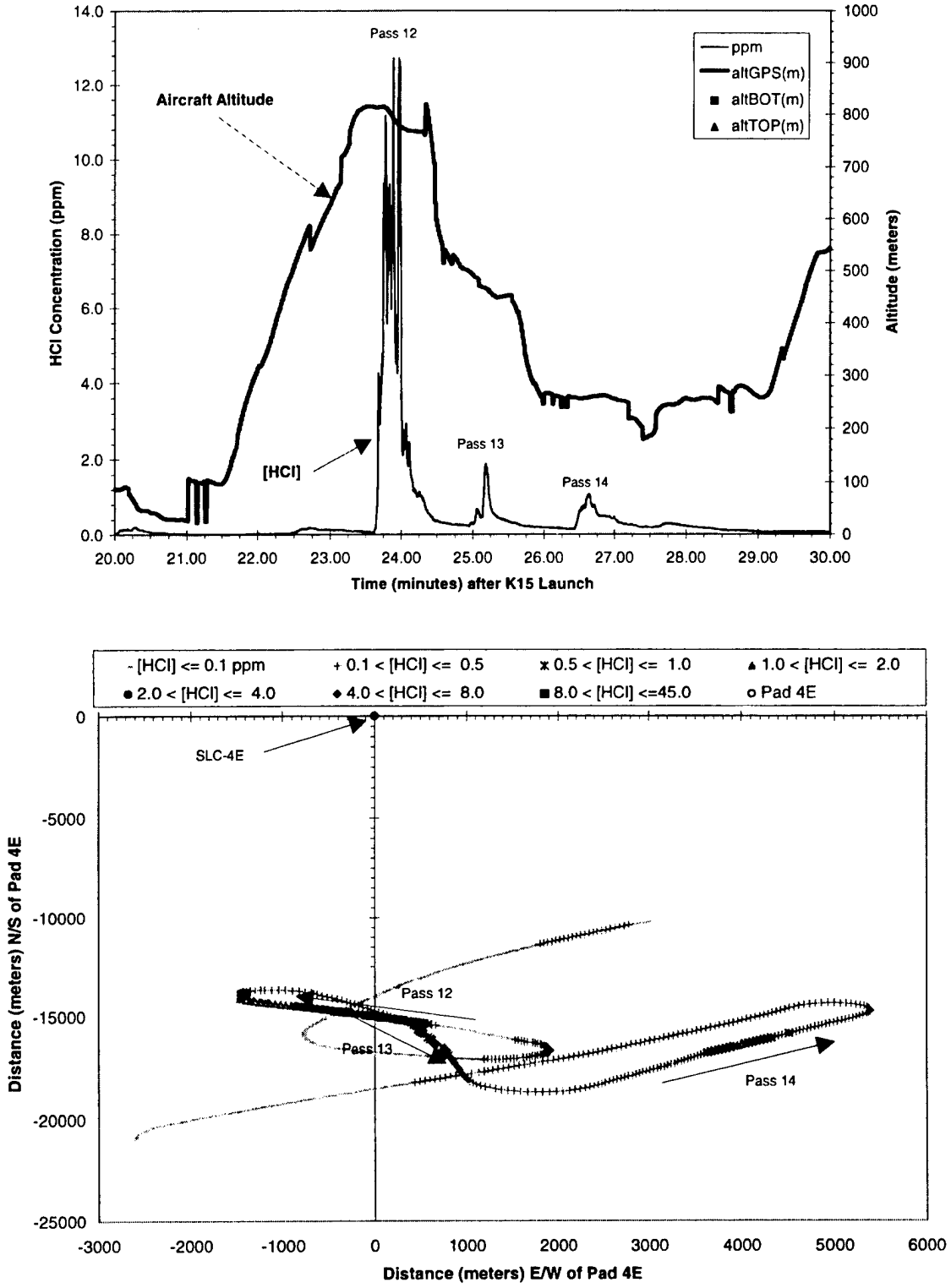

Figure B-3. Time and Cartesian Plots for Passes 12–14.

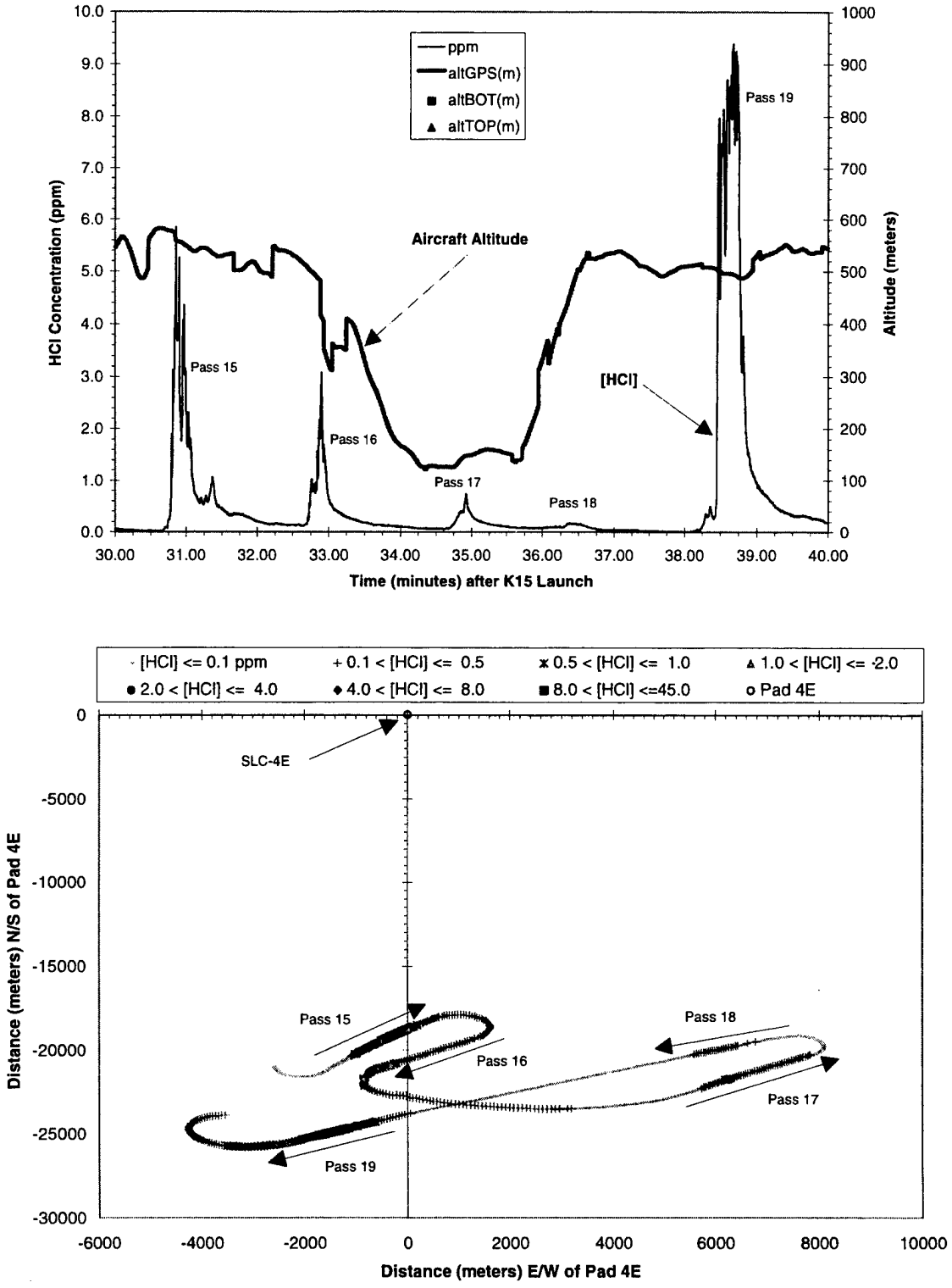

Figure B-4. Time and Cartesian Plots for Passes 15-19.

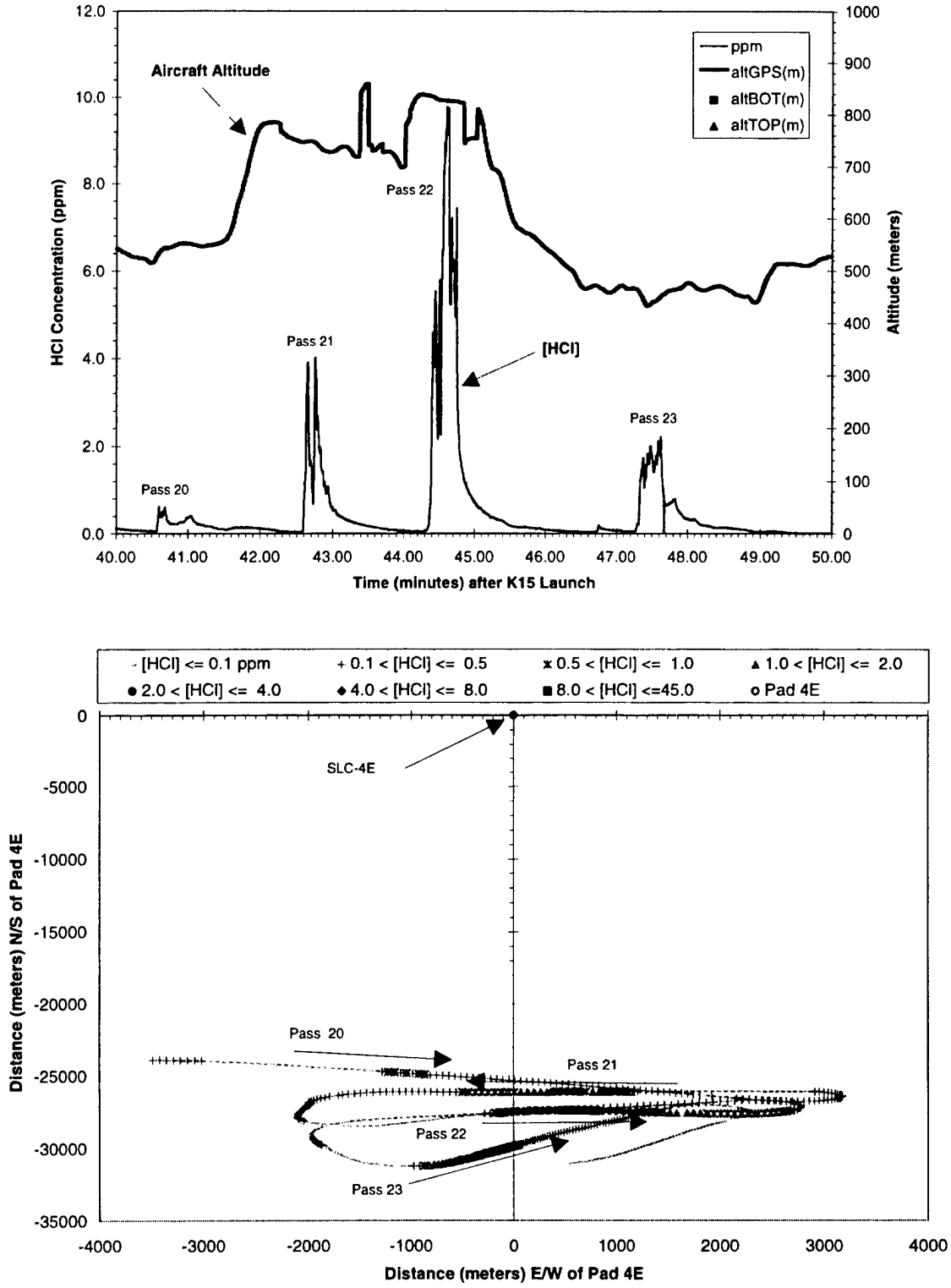

Figure B-5. Time and Cartesian Plots for Passes 20–23.

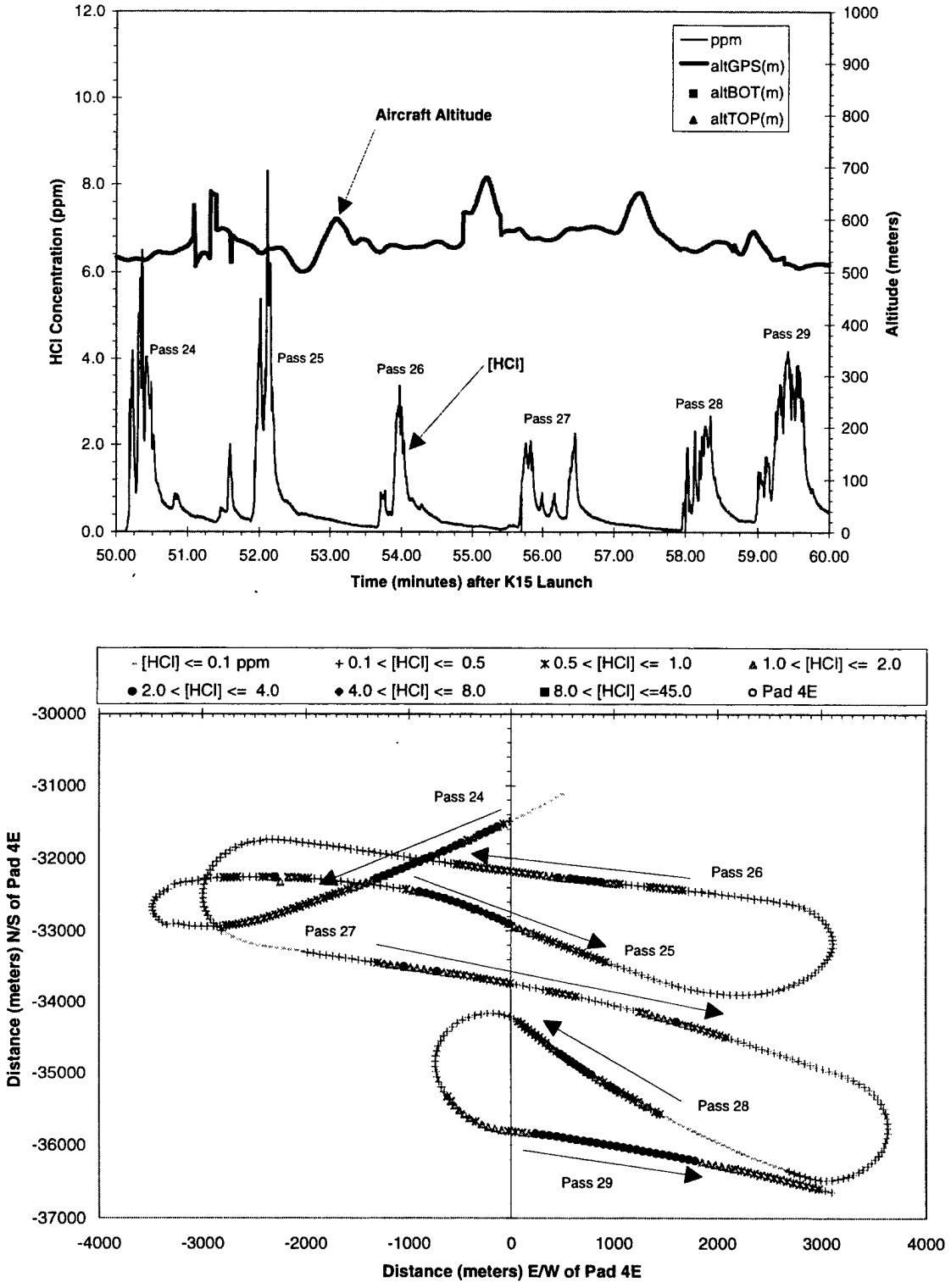

Figure B-6. Time and Cartesian Plots for Passes 24–29.

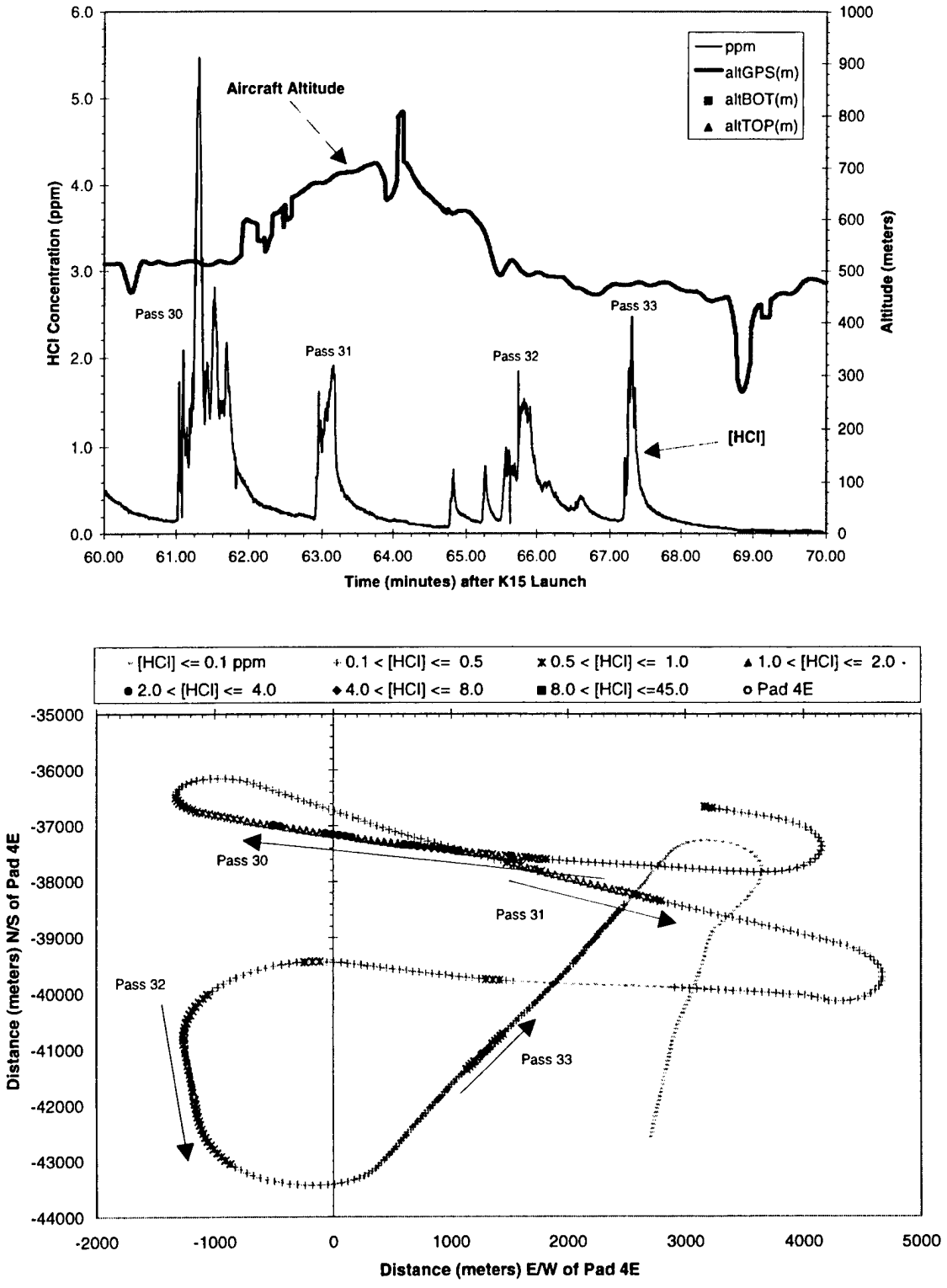

Figure B-7. Time and Cartesian Plots for Passes 30–33.

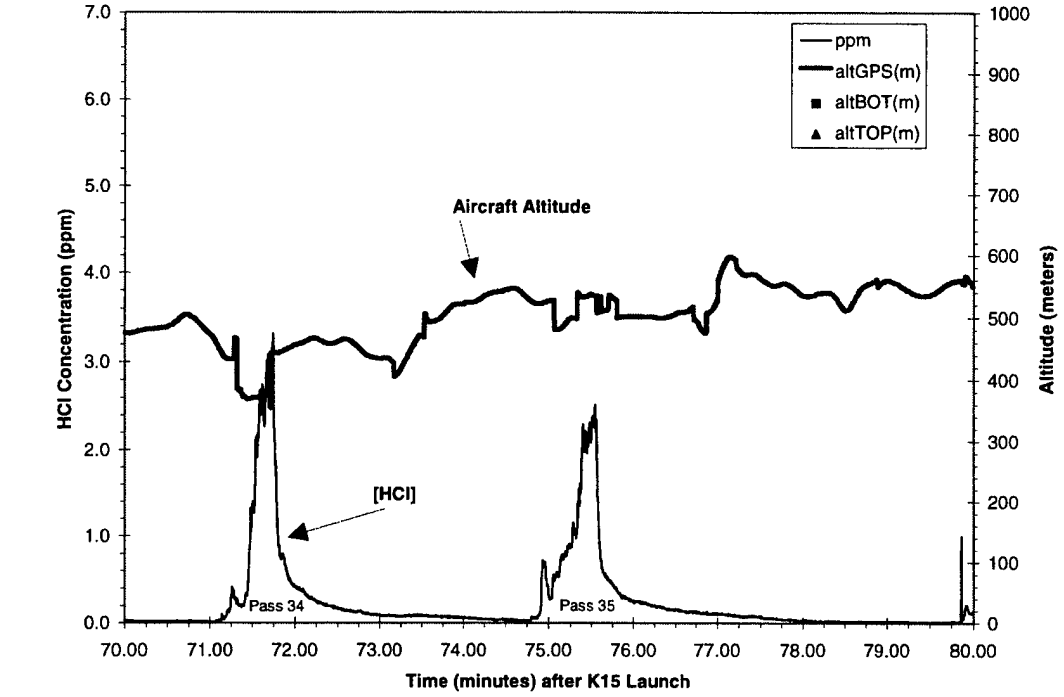

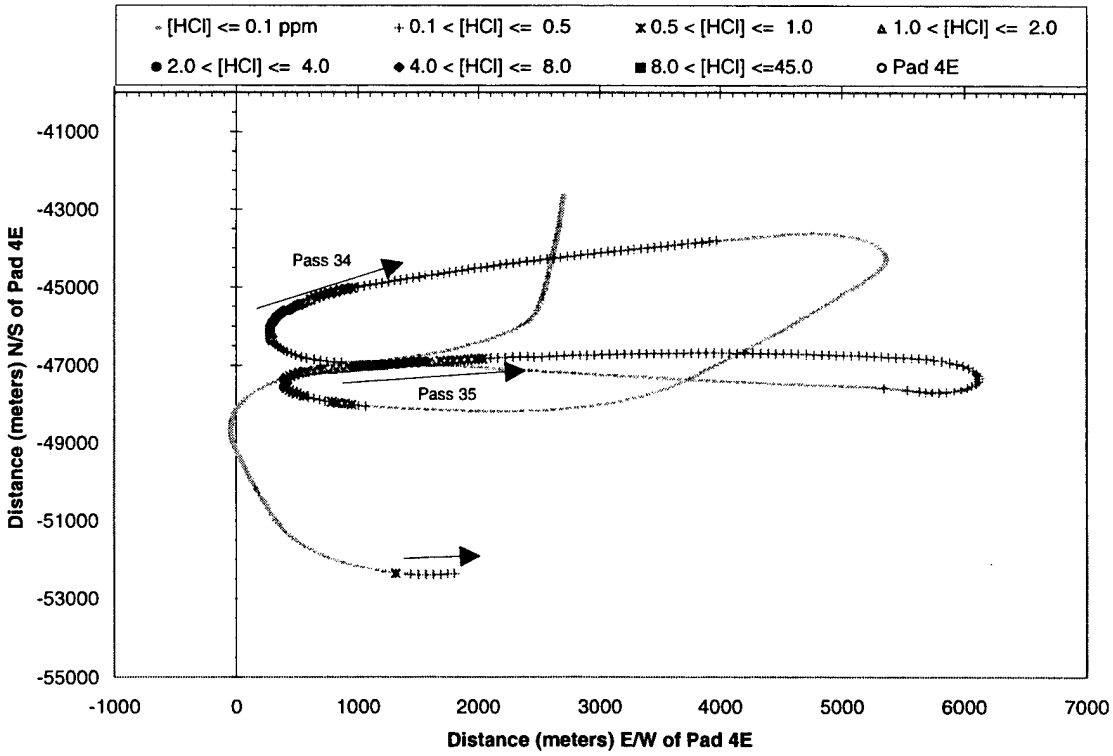

Figure B-8. Time and Cartesian Plots for Passes 34–36.

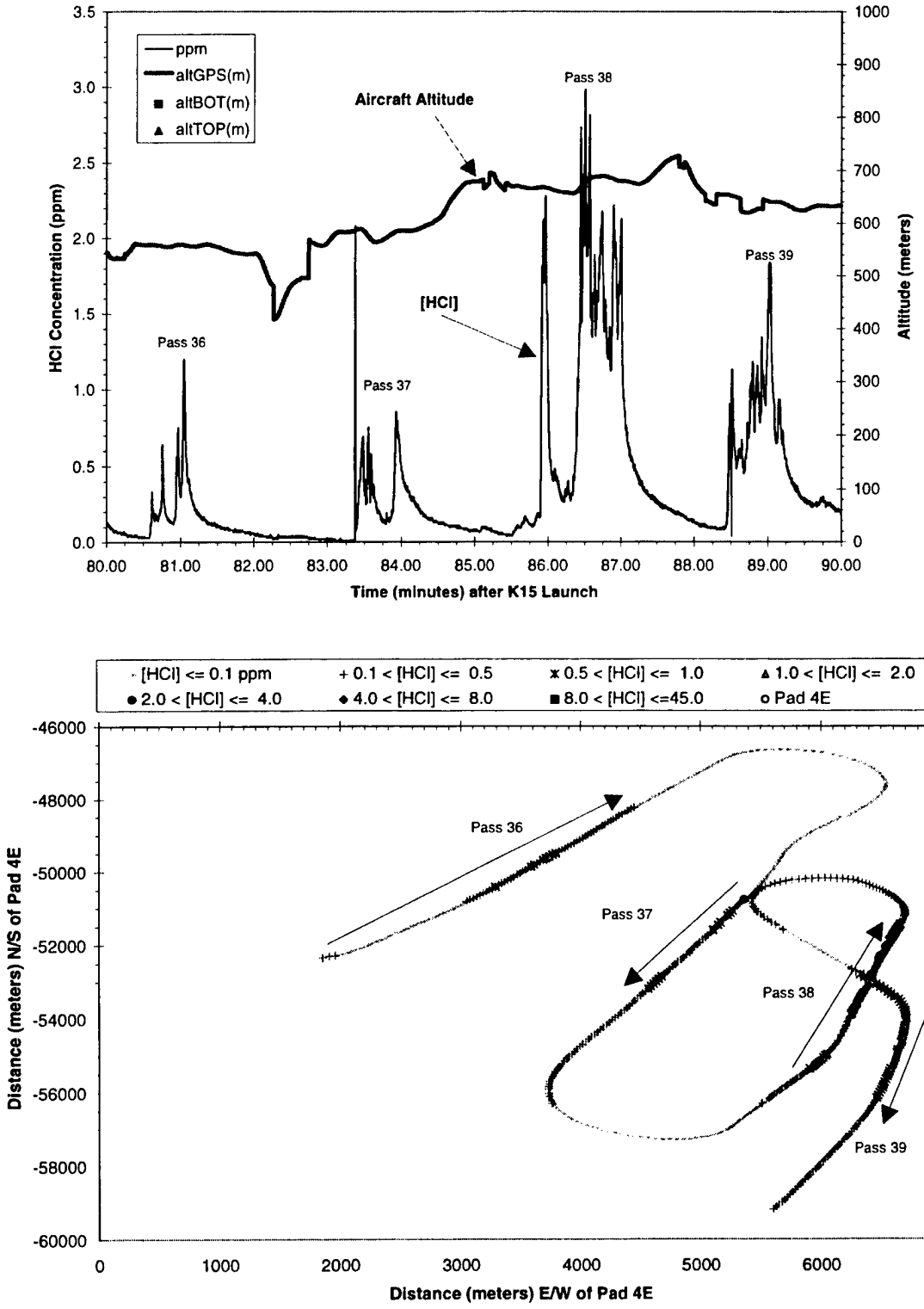

Figure B-9. Time and Cartesian Plots for Passes 36–39.

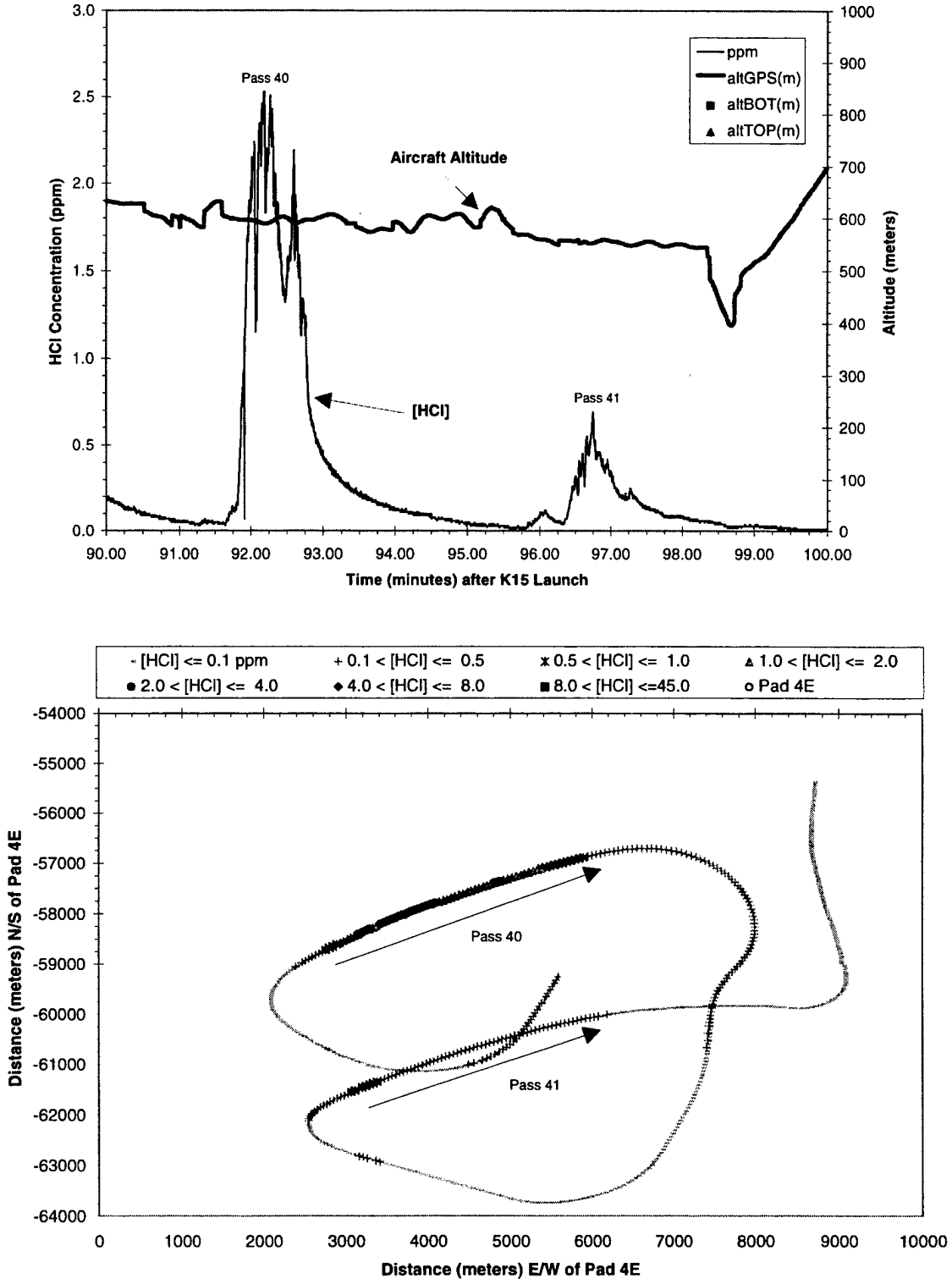

Figure B-10. Time and Cartesian Plots for Passes 40–41.

TECHNOLOGY OPERATIONS

The Aerospace Corporation functions as an "architect-engineer" for national security programs, specializing in advanced military space systems. The Corporation's Technology Operations supports the effective and timely development and operation of national security systems through scientific research and the application of advanced technology. Vital to the success of the Corporation is the technical staff's wide-ranging expertise and its ability to stay abreast of new technological developments and program support issues associated with rapidly evolving space systems. Contributing capabilities are provided by these individual Technology Centers:

Electronics Technology Center: Microelectronics, VLSI reliability, failure analysis, solid-state device physics, compound semiconductors, radiation effects, infrared and CCD detector devices, Micro-Electro-Mechanical Systems (MEMS), and data storage and display technologies; lasers and electro-optics, solid state laser design, micro-optics, optical communications, and fiber optic sensors; atomic frequency standards, applied laser spectroscopy, laser chemistry, atmospheric propagation and beam control, LIDAR/LADAR remote sensing; solar cell and array testing and evaluation, battery electrochemistry, battery testing and evaluation.

Mechanics and Materials Technology Center: Evaluation and characterization of new materials: metals, alloys, ceramics, polymers and composites; development and analysis of advanced materials processing and deposition techniques; nondestructive evaluation, component failure analysis and reliability; fracture mechanics and stress corrosion; analysis and evaluation of materials at cryogenic and elevated temperatures; launch vehicle fluid mechanics, heat transfer and flight dynamics; aerothermodynamics; chemical and electric propulsion; environmental chemistry; combustion processes; spacecraft structural mechanics, space environment effects on materials, hardening and vulnerability assessment; contamination, thermal and structural control; lubrication and surface phenomena; microengineering technology and microinstrument development.

Space and Environment Technology Center: Magnetospheric, auroral and cosmic ray physics, wave-particle interactions, magnetospheric plasma waves; atmospheric and ionospheric physics, density and composition of the upper atmosphere, remote sensing, hyperspectral imagery; solar physics, infrared astronomy, infrared signature analysis; effects of solar activity, magnetic storms and nuclear explosions on the earth's atmosphere, ionosphere and magnetosphere; effects of electromagnetic and particulate radiations on space systems; component testing, space instrumentation; environmental monitoring, trace detection; atmospheric chemical reactions, atmospheric optics, light scattering, state-specific chemical reactions and radiative signatures of missile plumes, and sensor out-of-field-of-view rejection.